Behind-Armour Debris - Modelling and simulation A literature review

Mats Hartmann

FOI-R--1678--SE
ISSN 1650-1942

Weapons and Protection
Base data report

June 2005

FOI is an assignment-based authority under the Ministry of Defence. The core activities are research, method and technology development, as well as studies for the use of defence and security. The organization employs around 1350 people of whom around 950 are researchers. This makes FOI the largest research institute in Sweden. FOI provides its customers with leading expertise in a large number of fields such as security-policy studies and analyses in defence and security, assessment of different types of threats, systems for control and management of crises, protection against and management of hazardous substances, IT-security an the potential of new sensors.

FOI
Defence Research Agency
Weapons and Protection
SE-147 25 Tumba

Tel: +46-8-5550 3000
Fax: +46-8-5550 4143

www.foi.se

Behind-Armour Debris - Modelling and simulation

A literature review

FOI-R--1678--SE
ISSN 1650-1942

Weapons and Protection
Base data report

June 2005

Issuing organization	Report number, ISRN	Report type
FOI – Swedish Defence Research Agency Weapons and Protection SE-147 25 Tumba	FOI-R--1678--SE	Base data report
	Research area code 5. Strike and protection	
	Month year June 2005	**Project no.** E2007
	Sub area code 51 Weapons and Protection	
	Sub area code 2	

Author/s (editor/s)	Project manager
Mats Hartmann	Gunnar Wijk
	Approved by
	Sponsoring agency Swedish armed forces
	Scientifically and technically responsible

Report title

Behind-Armour Debris - Modelling and simulation
A literature review

Abstract (not more than 200 words)

The ability to model behind armour debris (BAD) is important in assessment of vulnerability and lethality. It is very hard to find a suitable model, despite the well recognized importance of the phenomena.

A literature review of models and simulations of BAD is presented together with a short description of some hydrocodes and important concepts in numerical simulations. Many physical, empirical and statistical models handle only part of the problem; either target failure or BAD cloud characteristics. Numerical simulations have problems with fracturing of the target material. Numerical erosion is sometimes used to assess which computational cells that form BAD. The numerical simulations are often combined with a post processor to include the stochastic behaviour of the debris cloud.

It is concluded that this is a research field that still needs a lot of work, both experimentally and numerically, before the models are reliable and usable in or as pre-processors to vulnerability assessment.

Keywords

BAD, behind armour debris, fragment, spall, modelling, simulation, hydrocode, analytical, statistical, empirical, vulnerability, lethality, assessment, penetration, perforation

Further bibliographic information	Language English
ISSN 1650-1942	**Pages** 52 p.
	Price acc. to pricelist

Utgivare FOI - Totalförsvarets Forskningsinstitut - Vapen och skydd 147 25 Tumba	**Rapportnummer, ISRN** FOI-R--1678--SE	**Klassificering** Underlagsrapport
	Forskningsområde 5. Bekämpning och skydd	
	Månad, år Juni 2005	**Projektnummer** E2007
	Delområde 51 VVS med styrda vapen	
	Delområde 2	
Författare/redaktör Mats Hartmann	**Projektledare** Gunnar Wijk	
	Godkänd av	
	Uppdragsgivare/kundbeteckning Försvarsmakten	
	Tekniskt och/eller vetenskapligt ansvarig	

Rapportens titel (i översättning)

Splitter bakom skydd - Modellering och simulering
En litteraturstudie

Sammanfattning (högst 200 ord)

Möjligheten att modellera sekundärsplitter bakom skyddspaneler är viktigt i verkans- och sårbarhetsvärderingar. Trots det välkända behovet är det mycket svårt att hitta lämpliga modeller.

En litteraturstudie över modeller och simuleringar av sekundärsplitter presenteras tillsammans med en kort beskrivning av några numeriska beräkningsprogram och några, till beräkningsprogrammen, viktiga begrepp. Många av de fysikaliska, empiriska och statistiska modellerna hanterar endast en delmängd av problemet, antingen brottmekanismen i målet eller splittermolnets egenskaper. De numeriska simuleringarna har problem med brott i målmaterialen. Numerisk erosion används ibland för att bestämma vilka beräkningsceller som bildar sekundärsplitter. Ofta kombineras de numeriska simuleringarna med en postprocessor för att kunna inkludera det stokastiska uppträdandet hos splittermolnet.

Det konstateras att detta är ett forskningsområde som fortfarande kräver mycket arbete, både experimentellt och numeriskt, innan modellerna är trovärdiga och användbara i eller som underlagslämnare till värderingsarbeten.

Nyckelord

Sekundärsplitter, fragment, modell, simulering, analytisk, statistisk, empirisk, sårbarhet, verkan, värdering penetration, perforation, krossning

Övriga bibliografiska uppgifter	**Språk** Engelska
ISSN 1650-1942	**Antal sidor:** 52 s.
Distribution enligt missiv	**Pris: Enligt prislista**

Contents

1 Introduction

When a projectile or a shaped charge jet perforates a target plate there will often be a cloud of debris around the residual projectile behind the plate. These particles may hit and injure personnel or components inside an armoured vehicle.

To be able to predict the consequences of an attack one has to estimate the number of particles, their masses, velocities and directions in the cloud, as well as the residual velocity, mass and direction of the projectile. This need is recognized by numerous authors [1, 2, 3, 4] working with terminal ballistics applications. The task is illustrated in and Figure 1, where the black lines represent the impacting projectile and the behind-armour debris (BAD) trajectories inside an armoured fighting vehicle, and in Figure 2, where the numerous holes around the center hole are created by BAD. It is, despite the widely recognised need for the ability to model BAD, hard or impossible to find a good and simple model to use in more complex codes [5, 6]. The aim of this literature review is to give an overview of current knowledge of models for and numerical simulations of the contents and properties the debris cloud. These kinds of impact events are complex in terms of material deformation and thermodynamic state. Solutions have increasingly relied upon computational methods [1].

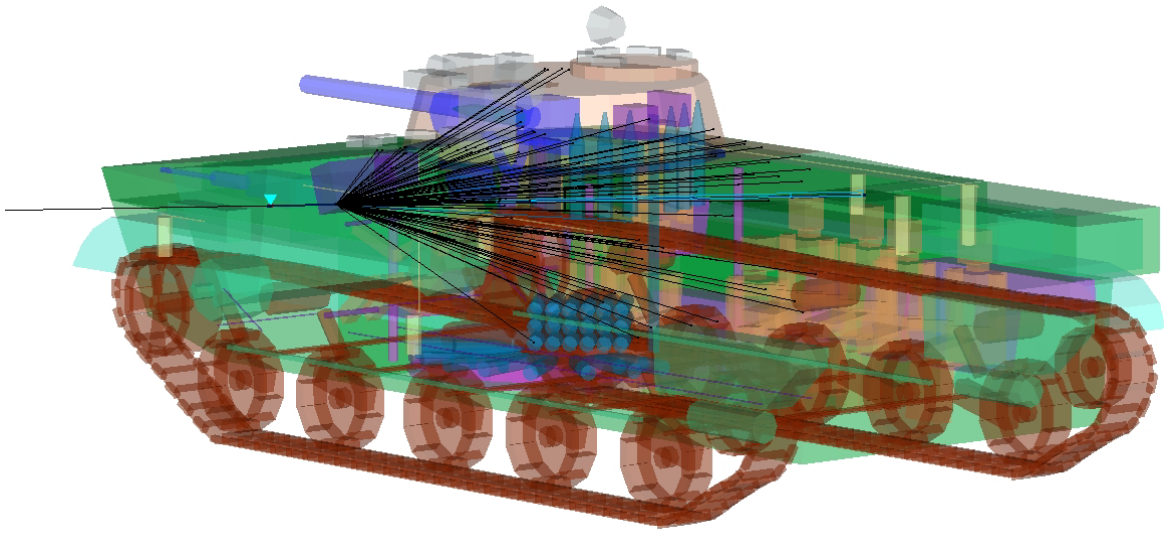

Figure 1: Illustration of the need of accurate BAD modelling where black lines represent the BAD trajectories.

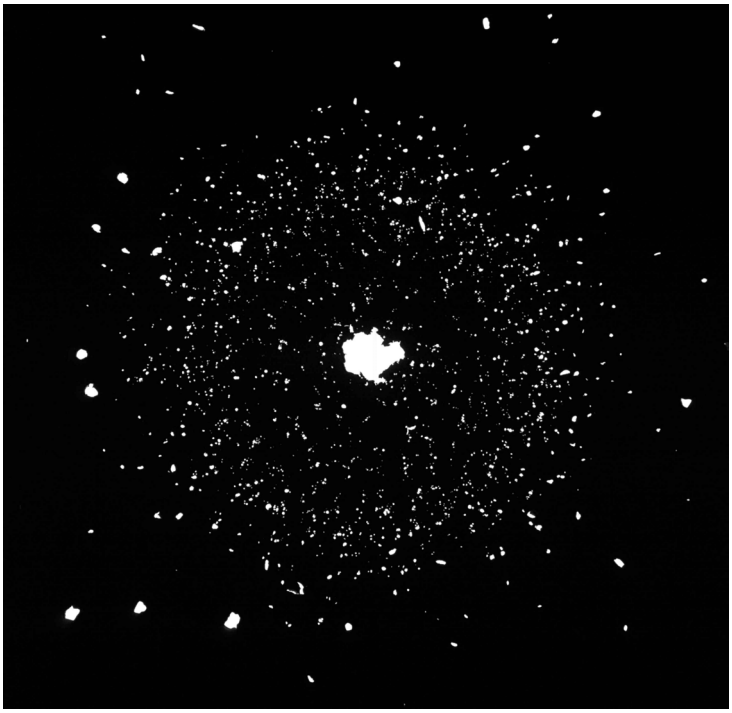

Figure 2: Example shoving the distribution of BAD in a target plate.

Conclusions from a previous literature review of this problem, presented by Dinovitzer *et al*, revealed [6]:

1. Additional work is still required in order to understand the underlying physics of BAD generation.
2. An integrated BAD characterisation and modelling process has not yet been fully developed.

Researchers have been working with the mission of understanding penetration and perforation mechanics for military purposes for long times. Many empirical and physical models have been presented, often with a statistical distribution of fragment sizes. During the last decades numerical calculations have increased in popularity.

2 Physical, statistical and empirical models

Models may vary from simple empirical relations to complex models that present systems of equations describing fracture initiation and growth as well as basic continuum mechanics equations. In the following sub-chapters some models with different focus will be presented.

2.1 Target failure and fragment generation

Either the projectile or the target has to fail and shatter in order to produce fragments behind the protective plate. The models in this section are focused on the generation of fragments and failure modes of the target plate.

An impressive literature review by Backman and Goldsmith, with references dating back to the 19th century, presents eight perforation mechanisms [7], of which four are presented in Figure 3.

1. Fracture due to initial stress wave
2. Radial fracture behind initial wave in a brittle target
3. Spall fracture (Scabbing)
4. Plugging
5. Petaling (frontal)
6. Petaling (rearward)
7. Fragmentation
8. Ductile hole enlargement

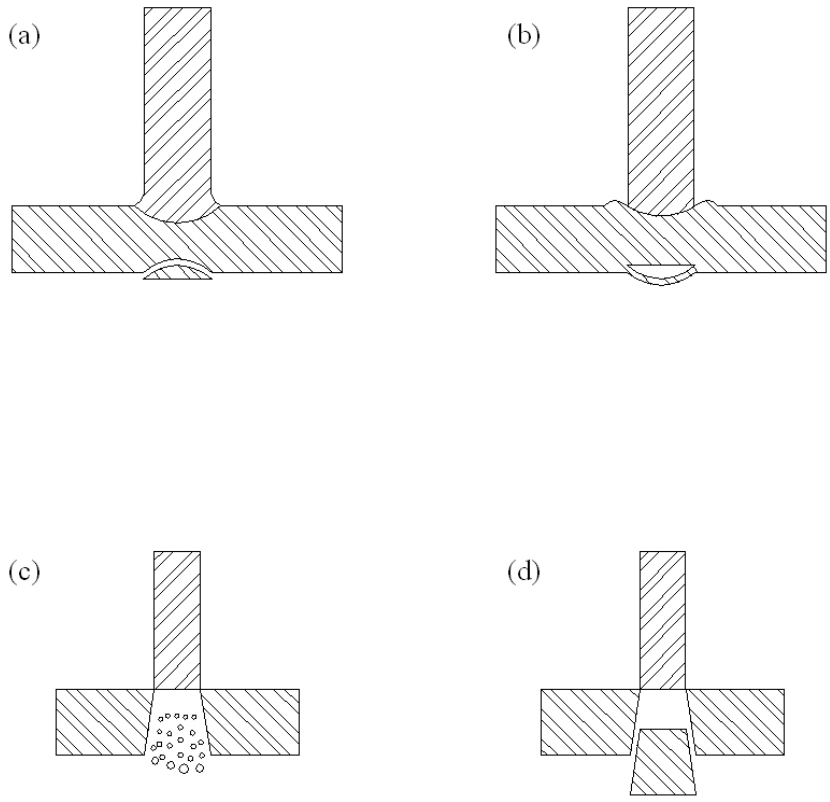

Figure 3: Perforation mechanisms [7]. Fracture due to (a) initial stress wave, (b) spall fracture or scabbing, (c) fragmentation and (d) plugging.

The term spalling will be used in many of the models described below. Spallation is a well known phenomenon to which entire books are devoted [8]. It should be noted that the definition of "spall"

may vary. Backman and Goldsmith [7] mean that "spalling is tensile material failure due to the reflection of the initial compressive wave from the distal side of the target and is a commonplace phenomenon under explosive loading". A slightly broader definition is given by Mescall and Papirno [9]: "Spallation in material refers to crack initiation and propagation resulting from a tension field induced by the interaction of stress waves". This definition is quite similar to the one given by Grady [13]: "Spall is the process of internal failure or rupture of condensed media through a mechanism of cavitation due to stresses in excess of the tensile strength of the material". One further definition of the term spall is given in [10], where a literature review of spall models is also found:" The term 'spall' refers to the internal material failure as result of cavitation due to dynamic stress waves" The dynamic waves originate from an impact and propagate trough the target. The compressive stress wave reflects from the back side of the target as a tensile wave. Whether or not spall occurs depends on the stress levels and the fracture toughness [10].

A common type of failure, often mentioned together with and with the same meaning as spalling, is scabbing. Backman and Goldsmith [7] define scabbing as: "Scabbing has a similar (to spall, author's comment) appearance, but the fracture is produced by deformation and its surface is determined by local inhomogeneiteis and/or anisotropies". Most other authors use spall and scab as synonyms.

It seems accepted that spallation in brittle materials is controlled by dynamic micro-crack propagation with plastic deformation, where the cracks eventually coalesce to form a spall plane [11]. In ductile materials spallation is dominated by localised elasto-plastic deformation around existing voids which grow and coalesce [11].

Many models of fragment formation consider an element of mass δM within a body under deformation (expansion due to shock wave after an impact). The mass δM is assumed to be sufficiently small so that the strain rate within the element is nominally uniform. It is also assumed to be large compared to the average mass of individual fragments, resulting from the spallation, which is of the order of ρs^3, where ρ is the density and s the average fragment "side" length [1].

Grady [12] presents a model of spalling based on energy balance. The model is developed for dynamic fragmentation in a fluid medium and later applied to more complicated materials. It is stated that the instantaneous thermodynamic and kinematical state of an expanding body of fluid is provided by the density ρ, the density rate $\dot{\rho}$ and the temperature θ. The kinetic energy associated with the outward motion is alone responsible for the fracturing forces, although most of the kinetic energy will remain after fracture when the newly formed particles fly apart. It is only the kinetic energy relative to the centre of mass (called local kinetic energy) that is available to fuel the breakage process. It is assumed that during the fragmentation process the forces brought about will seek to minimize the total energy density with respect to fractured surface area. The equilibrium fragment surface area to volumetric ratio, A, in terms of surface energy, density and density rate is then

$$A = \left(\frac{3(\dot{\rho})^2}{5\rho\gamma} \right)^{1/3}, \qquad (1)$$

which provides a quantitive measure of the fractured surface area in terms of fundamental thermodynamic and kinematical properties. After assuming that all fragments are equal and spherical with diameter

$$d = \frac{6}{A}, \tag{2}$$

and neglecting the stored elastic energy in brittle materials one obtains the nominal fragment diameter

$$d = \left(\frac{\sqrt{20} K_{IC}}{\rho c \dot{\varepsilon}} \right)^{\frac{2}{3}}, \tag{3}$$

where K_{IC} is the material fracture toughness, c the speed of sound in the material and $\dot{\varepsilon}$ the linear strain rate ($\dot{\varepsilon} = \dot{\rho} / 3\rho$). The prediction of Eq. (3) is compared with experimental data for oil shale and high-strength steel with reasonably good agreement.

In later work Grady [13] proposed two conditions that place constraints on the process of dynamic spall and determined inequalities which bound the spall strength, fragment size and failure time. The spall process in brittle solids is viewed as linear tensile, se Figure 4, loading until a critical spall stress, P_s, and fracture or spall time, t_s, at which point instantaneous failure is assumed to occur. It is assumed that each volume of size $\sim (c_0 t)^3$ fails independently, since at time t , referenced to the start of the tensile loading, the communication horizon (determined by the speed of sound, c_0) is not greater than $\sim c_0 t$.

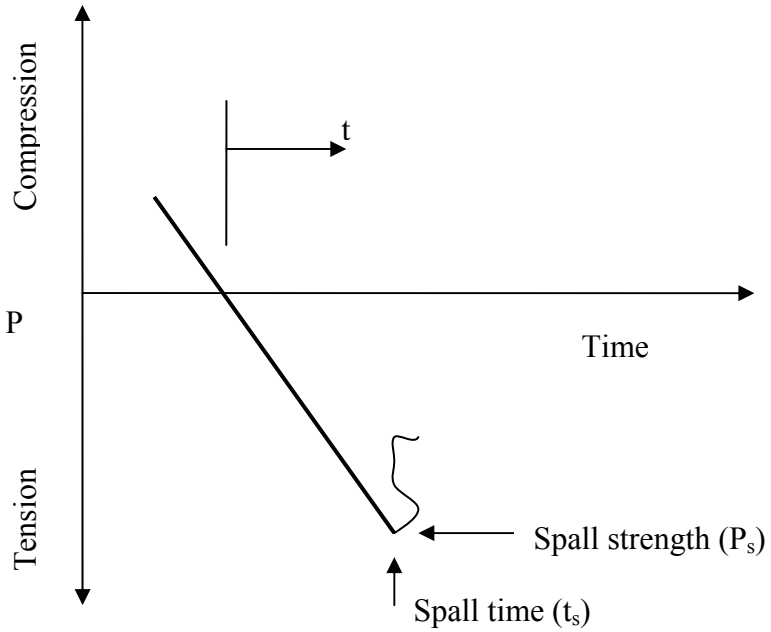

Figure 4: The spall process according to Grady [13]

Accordingly the average fragment size should satisfy

$$s \leq 2 c_0 t, \tag{4}$$

where the factor of 2 follows from geometric considerations of fracture sites on a rectangular lattice with cracks propagating to a radius of $c_0 t$ before coalescence. Eq. (4) is called the horizon condition and is the first criterion assumed to hold in the spall phenomenon [13].

The second criterion, which is called the energy condition, assumed to hold in the spall phenomenon [13] is

$$\frac{1}{2}\frac{P^2}{\rho c_0^2} + \frac{1}{120}\rho \dot{\varepsilon} s^2 \geq \frac{3K_c^2}{\rho c_0^2 s}, \tag{5}$$

where P is the stress in the expanding body, $\dot{\varepsilon}$ the linear strain rate and K_c the fracture toughness. The first term to the left in Eq. (5) represents an elastic energy density (which was neglected in [12]), while the second term represents the local kinetic energy within the body, available for fragmentation. The fracture energy per unit volume is to the right in Eq. (5), assumed that the body is broken into fragments of size s, a fracture surface area per unit volume equal to $6/s$ is created and that the fragments are equally sized spheres.

Since spalling is a specific kind of fracture, which is loading history dependent, the aspects of the initial microstructure and its evolution during plastic deformation are important [14]. Microscopic observations of cross-sections and spall surfaces have been performed by Klepaczko and Chevrier [14] using three scales: the micro scale, the meso scale and the macro scale. The observations confirmed that the spall process is a result of nucleation, growth and coalescence of micro-cracks during fracture of brittle materials and micro-voids when ductile fracture is more likely.

A model is proposed based on an elementary cell. The first step is nucleation of a micro-crack, which starts when the local stress exceeds the particle-matrix critical stress, σ_d, the decohesion stress. This stressfor a symmetric crack is determined by

$$\sigma_d = \sqrt{\frac{\xi E \gamma_R}{(1-\nu^2)a_c(t)}}, \tag{6}$$

where $\xi = \pi/2$ for a penny shape and $\xi = 2/\pi$ for a ribbon shape, E is the Young's modulus, ν is the Poisson's ratio, $2a_c$ is the length of the current micro-crack and γ_R is the surface fracture energy.

The micro-crack propagates at velocity $\dot{a}$ (assumed constant) up to attainment of its final length $a_{\max}$, under the constant effective local stress σ_d.

The growth and coalescence stage absorbs more energy and takes much longer time then the nucleation and propagation stages. In the model it is assumed that plastic deformation in the fully formed micro-shear band increases abruptly up to the critical value of shear deformation Γ_c, and from this instant the progressive cracking of the micro-shear bands starts. The progressive cracking is continued at constant velocity V until complete coalescence of two neighbouring micro-cracks. The plastic deformation in the shear band is given by

$$\Gamma_p = \frac{Vt}{\delta} \qquad \Gamma_c = \frac{Vt_c^*}{\delta} \tag{7}$$

and the strain rate

$$\dot{\Gamma}_P = \frac{V}{\delta} = const. \tag{8}$$

In the experimental study of Chhabildas *et al* [15] free-surface "pull back" velocity measurements were conducted at the impacted target specimen. This is well suited for accurate spall strength determinations, since the shocked material is referenced from a zero state of stress. An estimate of the spall strength S_m from the measured free-surface "pull-back" velocity Δu_{pb} is obtained by

$$S_m = \frac{1}{2}\rho_0 c_l \Delta u_{pb}, \tag{9}$$

where ρ_0 is the plate material density and c_l its elastic wave velocity. As the tensile wave propagates towards the target's free surface, the peak amplitude of the wave is partially attenuated by the elastic wave generated at the spall surface. This is corrected by a function ΔS which is related to the thickness of the spall plate. When the correction is added to Eq. (9) this yields an estimate for the spall strength S of the material at the spall plane

$$S = S_m + \Delta S. \tag{10}$$

Table 1 presents a summary of material properties presented in [15]:

Table 1: Summary of material properties

Mateial	Material density ρ_0 (g/cm^3)	Elastic Limit HEL (GPa)	Yield Strength Y_0 (GPa)	Impact Stress σ_f (GPa)	Spall Strength S (GPa)	Fracture Toughness K_c (MPa m^{½})	Normalized Spall Strength S/ρ_0 (GPa/(g/cm^3))
Tungsten (Sintered)	19.22	3.60	2.09	23.4	1.36	5-11	0.071
Tungsten (Alloyed)	17.20	3.0	1.80	15.8	1.76	5-11	0.102
Molybdenum	10.21	3.10	1.82	12.6	2.31	11-22	0.226
Ti 6AL-4V	4.42	2.30	1.21	13.6	5.08	70-80	1.149
Tantalum (S)*	16.66	1.50	0.75	19.3	6.23	-	0.374
Tantalum (Q)*	16.66	2.00	1.00	60.0	8.05	-	0.483
Aluminium	2.70	0.75	0.30	20.3	1.72	25-30	0.637
*S represents shock loading, Q represents quasi-isentropic loading.							

If the stress-strain relation of a material in tension is represented by $\sigma = \rho_0 c^2 \varepsilon$ then it can be shown, by calculating the work W done in tensioning the material until it fractures at a spall stress S, that

$$\frac{S}{\rho_0} = c\sqrt{\frac{2W}{m}}, \tag{11}$$

where m is the mass of the body and c is the wave velocity [15]. S/ρ_0 can then been seen as an indication of a material's ability to resist fragmentation.

Bless [16] recommends, based on another experimental study, that the spall criteria for RHA, RC 33, should be $\sigma_S = -60$ kbar. In the same report there are also results for Copper, SAE 1020 Steel, 4340 Steel, Nickel and 1100 Aluminium presented but in these cases, the recommendations for which value to use are not as clear as for the RHA.

It should be noted that there are indications that the pull back velocity may not be generally valid in determination of the spall strength. Chen *et al* [17] concluded that "…the traditional determination of spall strength without taking into account the stress relaxation due to the damage evolution on the spall plane is not valid for the experimental 'pullback' in general."

Fugelso and Bloedow, as presented in the revive of Backman and Goldsmith [7], also present estimates of target failure limits for some of the failure modes presented in Figure 3, due to impact by blunt nosed projectiles. Spalling failure due to the reflected tensile wave corresponds to the limit velocity

$$v_\Lambda = \frac{2\sigma_{Yt}\left(1+\left(\frac{h_0}{R_p}\right)^2\right)(1-\upsilon)}{Z\left((1-\upsilon)+2\upsilon\sqrt{1+\left(\frac{h_0}{R_p}\right)^2}\right)}, \tag{12}$$

where

$$Z \equiv \frac{(\rho_t c_{Dt})(\rho_p c_{0p})}{\rho_t c_{Dt} + \rho_p c_{0p}}, \tag{13}$$

and σ is stress, h target thickness, R radius, υ Poisson's ratio, ρ densities, c wave velocities and the subscripts Y, t, 0, p and D stands for Yield, target, original, projectile and dilatational, respectively. A condition that the radial stress at the rear surface is equal to the yield stress in tension is used to calculate the failure limit in Eq. (12) due to the tensile stress in the initial wave. The value of v_Λ is given by

$$v_\Lambda = \left(\frac{1-\upsilon}{1-2\upsilon}\right)\frac{\sigma_{YS}}{Z}\sqrt{1+\left(\frac{h_0}{R_p}\right)^2}, \tag{14}$$

for compressive failure on the rear side of the target due to the initial dilation wave.

This is based on an assumption that failure occurs when the maximum shear stress is equal to the yield stress.

It is possible that a plug, instead of many small fragments, is created during perforation of non-brittle target materials. An analysis developed to describe phenomenologically the plugging process occurring in thin plates or those of intermediate thickness is presented by Liss *et al* [18]. In this model plastic wave theory is employed to construct a five-stage penetration process that consists

sequentially of indentation, plug formation, separation and slipping, and post perforation deformation. The only projectile shape considered is a rigid flat-ended cylinder and the entire target is considered as a rigid/work-hardening material which is incompressible in the plastic domain.

The mechanisms involved in plugging penetration [18] are as follows:

1. Sideways erosion of material passing through the stationary shock layer produced just ahead of the projectile-target interface when the relative velocity exceeds the plastic shock wave velocity in the target.
2. Axial plastic wave propagation in the target zone ahead of the projectile. Material passing through this front is plastically deformed and instantaneously acquires the projectile velocity.
3. Material not yet reached by the plastic shock wave or that behind it acts as a rigid body, equivalent to the neglect of elastic strains.
4. A constant value of peripheral shear is assumed in a narrow annulus at the projectile boundary representing the adiabatic shear zones across which the velocity field is considered to exhibit a discontinuity.

The equations in [18] consider momentum conservation across the shock front as well as target reactive force and projectile deceleration. The model uses development of plastic hinges to describe deformation of the target, outside which the target is stationary and un-deformed.

One further model for plugging is presented by Pytel and Davids, [19]. Their study considers impacts of plates by projectiles under conditions which lead to failure of the plate by formation of a plug. The model is based on the following assumptions:

1. The plate response to the high stresses are of viscous nature (stress proportional to strain rate)
2. Vertical shearing stress is the only stress which needs to be considered and it is radially symmetric.
3. The vertical shearing is uniform across the plate thickness.

The model then gives equations for the shearing stress, the velocity field and displacements, caused by an impact represented as an initial velocity distributed over a circular area of the plate surface. Comparison with experimental results shows that the assumption of radial symmetry holds quite well, but the theoretical displacement field differs from that experimentally found outside the impacted area with increasing difference at increasing depth in the target [19]. The model predicts the displacements to gradually increase and approach infinity as time increases.

2.2 Debris cloud characteristics

The ability to describe the characteristics of the debris cloud that emerges behind the protective (armour) plate is at least as important as that of describing the fragmentation process. It is in fact the particles within the debris cloud that may cause injuries to personal in a fighting, no matter how they are created.

Verolme and Szymczak [20] present a semi-empirical/analytical model to determine the velocity and mass distribution in the debris cloud. Some commonly used basic assumptions are the following:

1. All debris particles are located on an expanding elliptical shell, according to Figure 5.
2. Impact takes place without yaw.
3. Every debris particle is spherical.

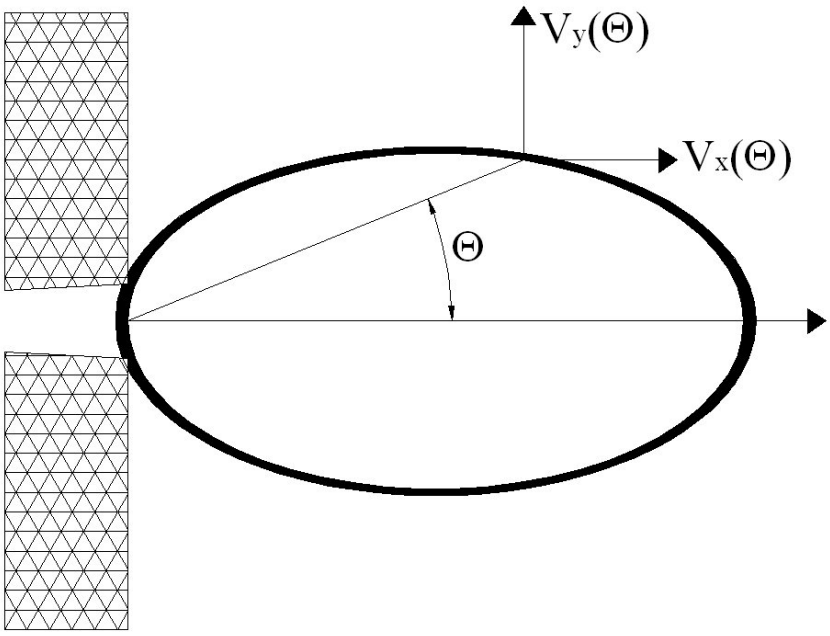

Figure 5: Assumed shape of BAD cloud [20]

The model is developed in connection with numerical simulations in AUTODYN. It is assumed that only 90% of the mass removed from the armour plate contributes to the BAD, to account for the front-splash and the lip fragments at the exit side. They estimate the average fragment size as

$$d = \left(\frac{\sqrt{24} K_{IC}}{\rho c \dot{\varepsilon}} \right)^{\frac{2}{3}}, \tag{15}$$

where K_{IC} is the dynamic material fracture toughness, ρ the density, c the speed of sound in the material and $\dot{\varepsilon}$ the linear strain rate. The estimate of d in Eq. (15) is almost identical to the Grady's estimate in Eq. (3). The average size is easily calculated since it is assumed that the fragments are spherical. The projectile deceleration by the target interaction is obtained from Newton's law of conservation of momentum

$$V_i - V_1 = \frac{\rho_T A_P}{2M_P} t_T V_i + \frac{R A_P t_T}{V_i M_P}, \tag{16}$$

where V_i is the projectile velocity before impact, V_1 the velocity after perforation, ρ_T the target density, A_P the projectile cross section area, M_P its mass, t_T the target thickness and R a parameter determining the target resistance.

A semi-empirical equation for the velocity distribution as a function of the emission angle θ is given:

$$V_x(\theta) = V_1 \cos(1.92\theta). \tag{17}$$

The spatial distributions of fragment mass and velocity can be obtained with Eq. (15) - Eq. (22), combined with the other equations given in [20].

According to Held [21] the term "secondary fragments" refers to fragments that arrive at a target component after one or more previous target plates have been perforated, irrespective if these fragments originate from the penetrator or the target plate. Others [22, 23] use "secondary fragments" solely for fragments from target plates. In these cases fragments from the penetrating object may be called "primary fragments".

The Held formula for fragment mass distribution [21], Eq. (18), is

$$m = M_0\left(1 - e^{-Bn^{\lambda}}\right), \tag{18}$$

where m is the summed-up mass of fragments, M_0 the total mass of fragments, n the summed up number of fragments, B a constant scaling factor and λ a constant form factor. Experimental results, where different types of secondary fragments (according to Held's definition) are separated, are compared to the Held formula in [21]. In order to get an optimum description of the fragment mass distribution it is usually needed to neglect some of the largest and possibly most dangerous fragments.

Further debris cloud distribution functions [24] are based on the experimental results in [25], where many illustrating photographs are presented as well as a phenomenological description of the debris cloud. During the perforation process a bulge is formed at the rear surface of the target. The bulge expands until it fragments and the debris are scattered behind the target. In [24] it was concluded that the best way to model the debris cloud is to assume that the outer boundaries of the expanding cloud are ellipsoidal. The target material is pushed in front of the eroding projectile and around its tip. It is therefore assumed that the target material is distributed on the cloud's outer surface while the eroded projectile material fills the inner ellipsoid volume. The front of the ellipsoid is assumed to move with the penetrator residual velocity and its rear part has a velocity which depends on target material properties. The model gives equations for the debris cloud geometry, based on the bulge height at the moment of breakage (for steel that is about four times the projectile diameter [25]), limiting angle beyond which no fragments will be found, velocity distribution and mass distribution. The model shows good agreement when compared to experimental results. Mayseless *et al* also discus the formation of ring fragments [24] of which the mass was excluded in the experimental results, whilst it was considered in the analysis of bulge dimension. The ring is assumed to be pulled out of the target in a process which is described as a stretching out of material, as illustrated in Figure 6.

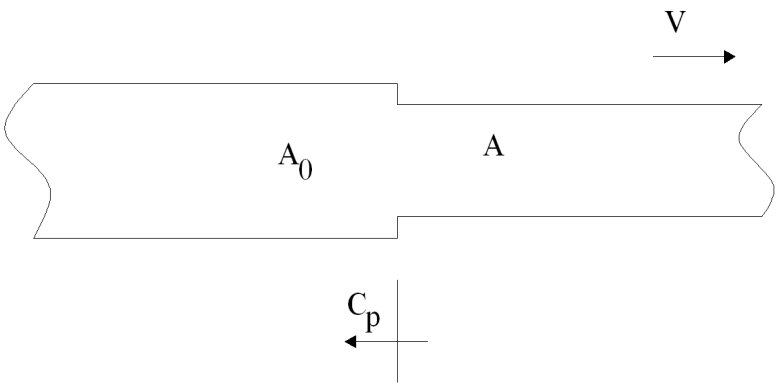

Figure 6: Scematic view of the streching mechanism in [24]

The condition for no change in volume gives

$$A_o C_p = A\left(V + C_p\right), \tag{19}$$

where C_p is the absolute plastic wave velocity and defines the rate of which te material is deformed. If the density ρ_0 is assumed constant the following expression can be obtained for the ring velocity [24]

$$V = \sqrt{\frac{Y}{\rho_0}}\sqrt{\frac{\varepsilon}{1+\varepsilon}}, \tag{20}$$

where Y is the material yield strength and ε the longitudinal tension engineering strain. The velocity that the extracted material gains depends on the amount of strain it can whithstand, and thus ductile material will produce greater ring velocities than brittle ones (given the same Y) [24].

Saucier *et al* present a stochastic model for the spall fragments behind an armour plate [26], following Mayseless *et al* [24]. The positions of the fragments are modelled as a truncated ellipsoidal shell. A velocity field of the fragments before and at the moment of break-up is given, with a virtual origin. After the break-up all fragments continue to have the same velocity as they had at the break-up moment and lay on the expanding truncated ellipsoid at any later time and move as though they originated from the virtual origin.

The stochastic properties enter the model in the fragmentation process. The fragments are modelled as parallelepipeds of side length a, b and c, where c is the thickness of the debris cloud shell, and the other two side lengths, a and b, drawn from a statistical distribution. Two distributions, Mott (or Weibull) and log-normal, are considered in [26]. In either case there are constants that have to be determined from experimental data. With assumptions of fragment sizes the resulting mass distributions are worked out, based both on the Mott and log-normal distribution.

Three major structural features of the debris cloud produced in conjunction with hypervelocity impacts are examined based on an experimental study by Piekutowski [27]. The presentation does not give a model for the debris cloud characteristic but describes the properties based on experimental results.

First, an ejecta veil, consisting almost of target material, was ejected from the impact side of the target. An expanding bubble of target debris was thereafter formed on the rear side. Finally, there was a significant structure composed of projectile debris located inside and at the front of the external bubble of target debris. When the debris clouds were compared on basis of similar *t/D* ratio (target thickness / sphere diameter) and impact velocity, the shapes of the morphological features and the internal structure were shown to be the same. Analyses of the fragment sizes indicated that the equivalent diameter of a large fragment along the centreline of the debris cloud scaled with the projectile diameter.

2.3 Combined models

This section presents some models that try to describe the complete process from impact to the produced debris cloud and the characteristics of the cloud.

An analytical impact energy conservation model employing fracture mechanics that predicts the expected number of fragments generated during ballistic penetration is presented by Dinovitzer *et al* [28]. The same model is also presented by Dinovitzer [10], where some experimental results used for calibration are also present. The model [28] was developed to describe medium calibre projectile's perforation of single or multiple layer metallic targets.

The model [28] tries to identify the relationship between the energy prior to and after a ballistic impact/penetration event. The energy which will promote fragmentation is the energy which remains after the penetration and target deformation processes are completed. The fragmentation energy, E_f, is expressed via an energy balance as

$$E_f = E_i - (E_d + E_p + E_1), \tag{21}$$

where E_i is the projectile impact energy, E_d the target debris kinetic energy, E_p the residual projectile kinetic energy and E_1 is the deformation and heating energy loss. Here it is assumed that the heating and deformation loss term is a function of the penetration energy. At impact velocities just below the penetration velocity (V_{50}) it is assumed that there will be no fragmentation, which is an approach that does not consider the potential for spall when no penetration occurs. The mass of the projectile is assumed to be constant and the energy possibly consumed for projectile break up is assumed to be a small fraction of the penetration energy. Then the amount of cracking, A_c, in the target plate is estimated based on the ratio of available fracture energy, E_f, and the rate of energy consumed per unit area crack growth, G, as

$$A_c = \frac{E_f}{G}. \tag{22}$$

This model also considers oblique ballistic penetration, unlike most other models. An equation for the mean number of fragments is given, under the assumptions that the fragments are cylindrical and with a geometrical description of a skewed elliptical cone [28, figure 2]. An equation that predicts the mean number of fragments is derived. The equation is evaluated for the mean values of each independent random variable (material toughness, fragments geometry, fragment mass and fragment velocity). The fragments are characterized as cylindrical elements.

A modelling process of probabilistic nature (basically the same model as in [28]) is presented by Dinovitzer *et al* [6]. This presentation is simpler than and thus not as complete as the one in [28]. It is summarized in three steps:

1. Identify the number of fragments from the fragmentation distribution.
   A random observation is drawn from a Weibull statistical distribution.
2. Sample fragment characteristic distribution.
   One observation is drawn for each fragment from the fragment mass, velocity, radial and angular location distributions.
3. Assemble fragment descriptions.

This can be completed once to give a deterministic result or multiple times to give a probabilistic description of the debris cloud.

In [29] a complete model of target fragmentation due to perforation by an eroding projectile is derived by Yarin *et al*. The model formulates equations describing the flow of material around the projectile. An energy balance, Eq. (23), gives an expression for the size of the smallest particle a_0

$$\frac{1}{2}\rho a_0^3\left(\dot{\varepsilon}\, a_0\right)^2 = \gamma a_0^2, \tag{23}$$

where ρ is the material density, a_0 is the diameter of the fragment, $\dot{\varepsilon}$ is the effective rate of strain and γ is the specific surface energy. The kinetic energy of deformation stands on the left in Eq. (23), and on the right, the surface energy. This model also gives a size distribution, estimate on the number of fragments created and their total mass via the so called "percolation theory". The percolation theory is applicable since the fragmentation process is random. The randomness in the model comes form the nucleus of lacunas (infinitesimal voids), which are distributed and orientated randomly. No fragment can leave the target until the fractured zone reaches the back surface. To solve the equations for fragment size distribution, total number and total mass, one has to know the shape of the fractured zone from which fragments are ejected through the targets back face. In [29] this zone is approximated by a cone, where the half angle at the origin changes with time as the projectile approaches the rear surface. The model does not handle the ring-like segments normally detached from the rear surface of the target, which may be a cause of the poor prediction of target mass loss when the model is compared with experimental results, but it does handle the fragmentation of the projectile. Even though the model is complicated mathematically (and is presented using tensor notation, which reduces the number of equations but makes them much harder to interpret) it has an attractive overall simplicity and completeness.

Wijk [30] presents a model that predicts the volume (or mass) of generated fragments as well as the debris cloud characteristics. First the total volume V of the fragments is determined as

$$\begin{aligned} V &= \frac{\pi D^2 h^*}{4} \qquad \text{when} \qquad h > h^* \\ V &= \frac{\pi D^2 h}{4} \qquad \text{when} \qquad h < h^*, \end{aligned} \tag{24}$$

where D is the hole diameter (equal to the projectile diameter if the projectile is rigid), h the target thickness. h^* is a transition thickness from the penetration process to the perforation process, whereby the projectile is assumed to crush the remaining material in front of it instead of moving it elastic-plastic radially.

The first assumption about the velocities of the fragments, the total volume of which is V, is that every fragment is ejected with the same velocity v_{exit} as the projectile has when it leaves the target. This velocity is derived by energy conservation and is

$$v_{exit} = \sqrt{\frac{mv^2 - 2W_{\min}}{m_{exit} + V\rho_T}}, \tag{25}$$

where m and v are the mass and velocity of the projectile at impact, m_{exit} the mass of the projectile when it leaves the target, $W_{\min}$ the energy used for penetration and ρ_T the density of the target material.

The ejected fragments are assumed to be distributed within a cone around the projectile's direction of motion. There is an angle Θ between the conical surface and the projectile's direction. It is assumed that the fragments are evenly distributed over a spherical surface with the radius $R = v_{exit}t$

inside the cone at a time t after the ejection. The half apex angle Θ of the cone and the number of fragments N are given by

$$\Theta = \Theta_0 + \Theta_1 (1 - \frac{v_{\min}}{v}), \tag{26}$$

and

$$N = \exp\left(\alpha \left(\frac{v}{v_{\min}} - 1 \right) \right). \tag{27}$$

Here Θ_0, Θ_1 and α are non-dimensional parameters that have to be determined via comparison with experimental results and $v_{\min}$ is the minimum impact velocity required for perforation. Wijk [30] also presents expressions for non-uniform distribution of the fragments within the cone and a mass distribution, where $M(\mu)$ is the accumulated mass of all particles with a larger mass than μ such that

$$M(\mu) = M_0 \exp(-\omega\mu). \tag{28}$$

Here is M_0 the total mass of all particles and ω a fragmentation number.

Wijk has observed that in most cases there are a few larger fragments among a large number of considerably smaller fragments. These few larger fragments were found at larger angles than the cone angle Θ. It is assumed that these particles are not created during the final perforation of the target, but are ejected as a result of elastic wave reflection from the rear surface of the target plate. These spall particles are assumed to be ejected with the velocity v_c, given by

$$v_c = \frac{2 c_T Y_T}{E_T}, \tag{29}$$

where c_T, Y_T and E_T are the elastic wave velocity, the yield strength and the elastic modulus of the target material. The model [30] is not compared with experimental results in such a way that it is verified and nothing can thus be said about its relevance.

2.4 Models for evaluation of witness plates

In many experimental studies witness plates are used to register the direction, size and velocity of the fragments in the BAD cloud. This section presents a model for such evaluation.

In [3] the mass, M_f, of the fragment creating a hole in a witness plate is determined in an iterative process which employs a shape factor K, the hole area A and a plate hole diameter ratio γ (hole diameter / fragment diameter) as

$$M_f = \left(\frac{A}{\gamma K} \right)^{3/2}, \tag{30}$$

based on experiments with witness plates.

Here it assumed that the shape factor K also incorporates information regarding the fragment material density, ρ_f. It is assumed that the fragments are cylindrical, and once the mass has been identified the geometric characteristics (length, L_f, and diameter, D_f) can be estimated as:

$$L_f = \frac{M_f \gamma^2}{A \rho_f} \tag{31}$$

and

$$D_f = \sqrt{\frac{4A}{\pi \gamma^2}} \tag{32}$$

respectively. A minimum fragment velocity is derived based on how many witness plates the fragment was able to perforate. In doing this the cumulative kinetic energy required to penetrate multiple plates is estimated by summing the energy needed to perforate one plate. The non-dimensional ratios presented in Table 2 were analyzed.

Table 2: Analyzed non-dimensional ratios.

Relative Velocity	V_r	Fragment Velocity / Projectile impact velocity
Relative Mass	M_r	Fragment Mass / Projectile Mass
Relative Radial Location	R_r	Fragment Radial Location / Distance From Target

When the statistical data were reviewed it was found that Weibull and lognormal distributions were the most appropriate distributions.

It is shown by Merzhievsky in [31] that the hole diameters (and hence fragment sizes) in a witness plate behind a target plate subjected to hypervelocity impact can be described by the Rosin - Rammler (or Weibull) law. The model gives a probability density function of fragment size distribution.

In the experimental part of the study a thick duralumin was used as target for measuring the crater diameters and thinner shields were used to get the maximum fragment velocity v_1 behind the shield. Finally it is found that v_1 can be given by

$$v_1 = \frac{\sqrt{v^2 - v_b^2}}{1 + \eta}, \tag{33}$$

where v is the impact velocity, v_b an empirical function of the limit target thickness and η a function of densities and thicknesses.

3 Numerical methods

A computer program that uses finite difference, finite volume or finite element techniques to solve non-linear problems is often referred to as a "hydrocode" [32]. The phenomena to be studied with such a program, in the scope of this literature review, can be characterized as highly time dependent with large strains and stresses (geometric non-linearity) and plasticity, failure, hardening and softening, and multiphase equation of state (material non-linearity).

A key interest in developing advanced simulation tools (computer codes and material models) can be to examine a range of parameter variation of a protection configuration (materials, spacing, layers and threat) [33], even at impact velocities too great for experimental studies. Analysis and simulation with hypervelocity impacts are required for protection of e.g. space vehicles.

3.1 Important concepts in numerical simulations

There are a few expressions that often occur in connection to numerical simulations. Short descriptions of some of these expressions are given in the following section.

3.1.1 The finite element method

The finite element method is a numerical procedure for analyzing structures and continua [34], which originated as a method of stress analysis. Today it is also used to analyze problems of heat transfer, fluid flow, electric and magnetic fields and many more. A definition of the finite element method may be [34]: "a method of piecewise approximation in which the approximating function ϕ is formed by connecting simple functions, each defined over a small region (element). A finite element is a region in space in which a function ϕ is interpolated from nodal values of ϕ on boundary of the region in such a way that interelement continuity of ϕ tends to be maintained in the assemblage".

The power of the finite element method is its versatility. The method can be applied to various physical problems and it has a close physical resemblance between the actual structure and its finite element model. The numerical methods also have disadvantages. A specific numerical result is found for a specific problem: it provides no closed-form solution that permits analytical study of the effects of changing parameters. Experience and good engineering judgement are needed in order to define a good model; the extensive documentation of a general purpose program can not be ignored.

Depending on the unknowns and dependent variables the method can be qualified with words like *displacement, force, hybrid* or *mixed* [35].

3.1.2 The finite difference method

The finite difference method is a method in which a numerical solution of the differential equation for displacement or stress resultant is obtained for chosen points on the structure, referred to as nodes or pivotal points [36]. The numerical solution is then obtained from differential equations which are applicable to the actual continuous structure. This is different from the finite-element method, in which the actual continuous structure is idealized into an assembly of discrete elements. The numerical solution by finite differences generally requires replacing the derivatives of a function by difference expressions of the function at the nodes. The differential equation governing the displacement (or stress) is applied in a difference form at each node, relating the displacement at the given node and nodes in its vicinity to the external applied load. The finite-difference

coefficients of the equations applied at nodes on, or close to, the boundary have to be modified, compared to the coefficients used at interior points, in order to satisfy the boundary conditions. Therein lies one of the difficulties of the method and a disadvantage in its use compared with the finite element method.

3.1.3 The finite volume method

This is a numerical model for solving partial differential equations that calculates the values of the conserved variables averaged across the volume [37]. It does not require a structured mesh which is an advantage over the finite difference method. The values of the conserved variables are located within the volume element, not at the surfaces or nodes. This makes it possible that boundary conditions can be applied noninvasively [37]. These kinds of methods are powerful in calculations where the mesh moves to track interfaces of shocks.

3.1.4 Problem formulation techniques

A formulation technique must be chosen when a problem is defined in a hydrocode if the code allows more than one technique. Many codes allow the user to use different techniques in different parts of the problem definition.

3.1.4.1 Lagrangian formulation

A Lagrangian coordinate system, in which the coordinates move with the material, is suitable for following the flow in regions of relatively low distortions and possibly large deformations [32]. The Lagrangian coordinate system will deform with the material and therefore accurately define material interfaces, as shown in Figure 7. The history of the state of the material in a cell is known completely. Compared to the Eulerian method the Lagrange method tends to be faster computationally as no transport of material through the mesh needs to be calculated. Material interfaces, free surfaces are generally easier to follow with a Lagrange formulation than with an Eulerian formulation. A major drawback of the Lagrangian formulation is that if excessive material movement occurs, the numerical mesh may become highly distorted leading to an inaccurate and inefficient solution. The numerical mesh can be remapped to a more regular mesh to reduce the mesh distortion problem. Other techniques such as (numerical) erosion can also be used [32].

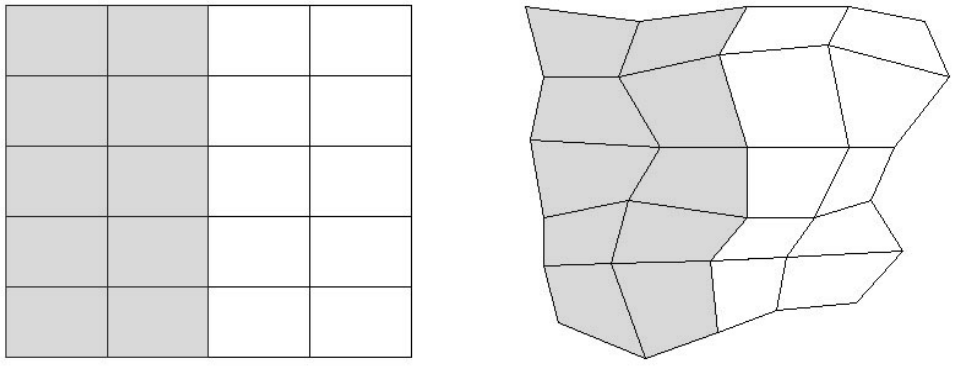

Figure 7: Undeformed (left) and deformed (right) Lagrange coordinate systems. The different shadings represent different materials.

3.1.4.2 Eulerian formulation

In Eulerian codes the material flows through the mesh [38]. This is often done in two steps or phases. In the first step (Lagrangian phase), the mesh is allowed do deform as the problem is

advanced in time and then, in the second step (advection phase), the distorted mesh is remapped back to the original mesh. The material interfaces are not well defined in Eulerian codes, as seen in Figure 8, due to the material flow through the mesh. The interface between two dissimilar materials is known at best to within some fraction of a cell dimension. These interface cells contain materials of both the bodies involved in contact and therefore are designated as "mixed cells" [38]. Today most Eulerian hydrocodes use a material interface reconstruction scheme. Even with a perfect material reconstruction algorithm, problems may occur when two material boundaries of the same material come in contact. In this case the interface can simply disappear, and the materials behave as one material [38].

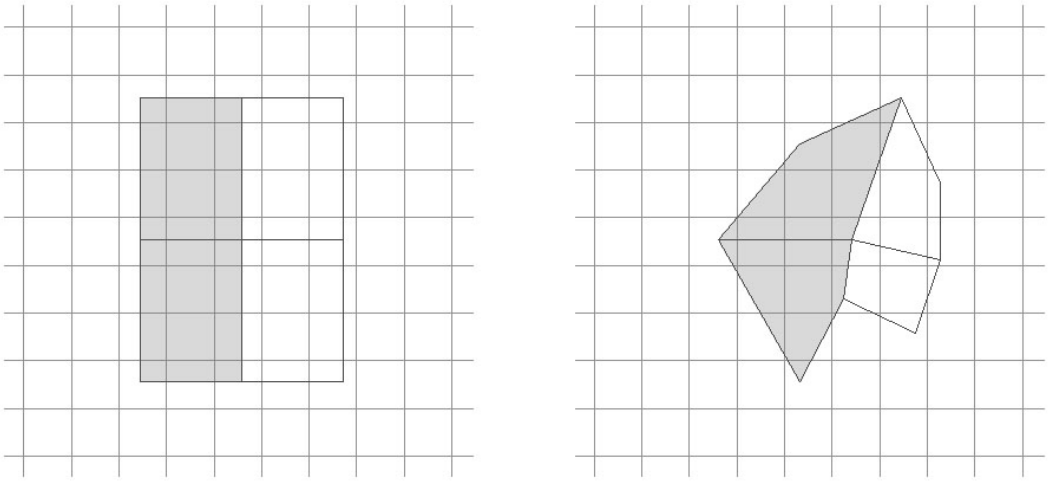

Figure 8: Undeformed (left) and deformed (right) body in Eulerian formulation.

A summary of advantages and disadvantages with Lagrangian and Eulerian formulations, [39], is presented in Table 3.

Table 3: Advantages and disadvantages of Lagrange and Euler formulation [39]

Advantages

Lagrange	Euler
• Clear definition of material borders • Information of load history • Sharper mapping of shock waves • Simpler program code • Shorter calculation times	• No net distortion • Possibility of material mixture • Larger deformation possible • Flow calculation possible

Disadvantages

Lagrange	Euler
• Small cells lead to small time steps and longer calculation times • Cell distortion may cause program abort	• Requires more calculation time • Material borders may be unclear • Needs finer net • Less adequate description of strength variation in time.

3.1.4.3 ALE (Arbitrary Lagrangian-Euler)

The ALE method is an extension of the Lagrangian method that, via additional computational steps, moves the grid and remaps the solution onto a new grid [32]. One promise of this technique is that

the freedom in dynamically defining the mesh configuration should allow a combination of the best features of both Lagrange and Euler.

3.1.4.4 SPH (Smooth Particle Hydrodynamics) formulation

The SPH technique uses no grid, it is a pure Lagrangian particle method [40]. The absence of a mesh and the calculation of interactions among particles based on their separation alone means that large deformations can be computed. A foundation of the SPH technique is interpolation theory. The conservation laws are transformed from partial differential equations into integral equations through the use of an interpolation function that gives the "kernel estimate" of the field variables at a point [40]. The reason why an underlying grid is not needed is that functions are evaluated using their values at the discrete points (particles) and an interpolation kernel.

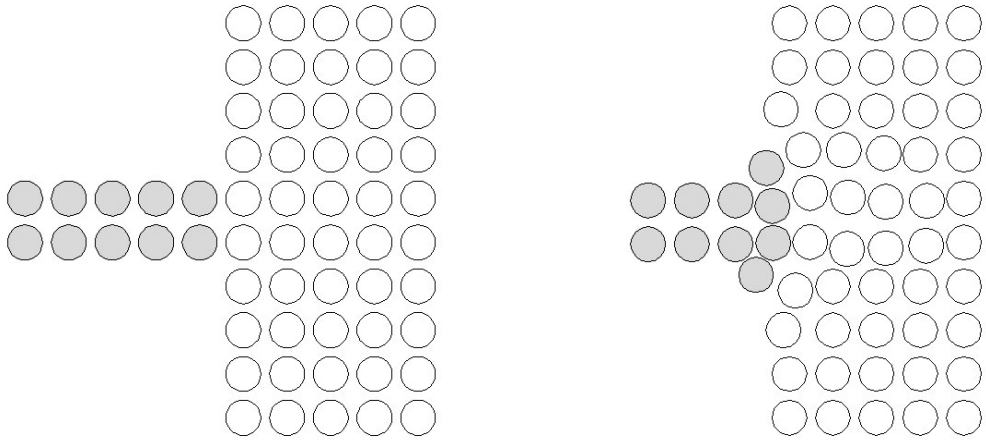

Figure 9: Undeformed (left) and deformed (right) bodies in SPH formulation.

3.1.4.5 Molecular Dynamics

Despite differences in computer realization, both Lagrangian and Eulerian techniques concern the same physical model based on the Navier-Stokes equations [41]. The principal assumptions of this model are: mass, momentum and energy flow continuity and thermodynamic equilibrium in differential volume. These assumptions fail for at least two important cases:

1. Investigations of microscopic mechanical properties of materials.
2. When the material considered is brittle, porous and the kinetic energy of the projectile is transferred mainly into mechanical energy of the target not changing the material properties.

These problems can be reduced by using the molecular dynamics approach. In the micro scale the material has to be seen as an ensemble of separate particles. In this scale the assumptions concerning matter, momentum and energy flow continuity and thermodynamic equilibrium in differential volumes are not longer valid [41]. Instead of Navier-Stokes based models, molecular dynamics have to be used. The principels and assumptions of one [41] computational model with molecular dynamics (MD) can be summarized as:

1. Both target and projectile are composed of particles.
2. Particles interact via short range potential.
3. Particle moves according to the Newtonian laws.
4. The model is two-dimensional.

With MD it is possible to simulate discontinuities like cracks and fragmentation of matter, in a way that is not allowed by continuous hydrocodes [41].

3.1.4.6 Other methods

There are other meshless methods than SPH, for example the 'diffuse element method' (DEM) and 'element-free Galerkin' (EFG), which uses moving least square approximations [42]. No user of these methods interested in fragment generation during projectile perforation of target plates has been found, so no further description of them will be given.It should be noted however that the EFG method can be used for fracture and crack problem simulations [43, 44], both statically and dynamically, which may be of use for simulation of fragments generated during perforation.

There are also hybrid models. One described in [45] employs particles and elements everywhere. The simultaneous use of particles and elements is not redundant, since they are used to represent distinct physics. The particles model all inertia and contact-impact effects, while the elements model all strength effects.

3.1.5 Equation of State (EOS)

The bases of most hydrocodes (except for codes for MD) are the three conservation equations [46]:

1. Conservation of mass
2. Conservation of momentum
3. Conservation of energy

Hydrocodes utilize differential equations for material dynamic motion to express the local conservation of mass, momentum and energy. To be able to obtain a complete solution, also considering initial boundary conditions, it is necessary to define a further relation between the flow variables. This can be found from a material model which relates stress to deformation and internal energy. It is, in most cases, possible to separate the stress tensor into a uniform hydrostatic pressure and a stress deviatoric tensor associated with the resistance of the material to shear distortion. This relation between the hydrostatic pressure, the local density (or specific volume) and local specific energy (or temperature) is known as an equation of state (EOS) [32].

An EOS can be expressed either by an analytic equation (or several equations), or by a table of numbers.

Much work has been done to describe models for different materials, since each material requires its own EOS. The more complex the material is the more complex the model will become. There may be a need of a set of EOSs if the material may undergo phase changes during the simulation.

One example of phenomena [47], believed to be of primary interest, when developing a model for highly anisotropic materials, in this case Nextel and Kevlar-epoxy, is [47]:

1. Shock response
2. Material compaction (particularly in Nextel which is macroscopically porous)
3. Phase changes (particularly epoxy vaporisation)
4. Material anisotropy
5. Anisotropic strength degradation
6. Coupling of volumetric and deviatoric response.

The anisotropy, porosity and complex failure mechanisms could be neglected if the material being modelled is aluminium.

The only practical way of obtaining data on the behaviour of the material at high strain rates is to carry out well-characterized dynamic experiments [32].

3.2 Hydrocodes

A short description of some of the hydrocodes that are used for simulations of behind armour debris will be given below. An more extensive survey of codes is presented by Post [48].

3.2.1 AUTODYN

The AUTODYN programs are general-purpose engineering software packages that use finite difference, finite volume and finite element techniques to solve non linear problems in solid, gas and fluid dynamics [32]. AUTODYN are released in both 2D (from 1986) and 3D versions (from 1991). AUTODYN employs a coupled methodology to allow a numerical solution for a given problem. Different domains of a physical problem can be modelled with different numerical techniques most appropriate for that domain. The code then couples these domains together in time and space to provide a solution. AUTODYN includes the following numerical processors [32]:

1. Lagrange processor for modelling solid continua and structures.
2. Euler processor for modelling fluids, gases and large distortions.
3. ALE (Arbitrary Lagrange Euler) processor for specialized flow models.
4. Shell processor for thin structural elements
5. SPH (Smooth Particle Hydrodynamics)

All the numerical processors use explicit time integration. Libraries of material data are included. AUTODYN is a product marketed by Century Dynamics.

3.2.2 EPIC

The EPIC-2 and EPIC-3 codes were originally developed during the mid seventies [49]. The abbreviation EPIC stands for “Elastic Plastic Impact Computations”. EPIC is a Lagrangian finite element code, and it has several options available for the material description [50]. During later developments an automatic rezoning algorithm has been implemented [51]. The rezoning maintains material mass and volume, unlike some erosions algorithms, and thus allows continued simulation of failed material.

3.2.3 CTH

CTH is a software developed to model multidimensional, multi-material, large deformation and strong shock wave physics [52]. A two-step Eulerian solution scheme is used. The first step is a Lagrangian step in which the cells distort to follow the material motion and the second is re-mesh step where the distorted cells are mapped back to the Eulerian mesh. A special model, useful for analyzing fragmentation experiments and witness plates, is available for moving fragments smaller than a computational cell with statistically correct velocity [52]. CTH was developed at Sandia National Laboratories.

3.2.4 LS-DYNA

LS DYNA is a general purpose transient dynamic finite element program capable of simulating complex problems [53]. The code is capable of simulating projectile penetration, blast response and

explosives (LS-DYNA's predecessor was originally written for military simulations). Among other capabilities probabilistic analysis is included in the code.

LS-DYNA is a product of Livermore Software Technology Group.

3.2.5 MESA

MESA is a 3D, Cartesian mesh, Eulerian code with hydrodynamics, high explosives and material strength models [54], developed specifically for simulations of armour and anti-armour systems. The hydrodynamics is divided into two parts. The first phase is a pure Lagrangian calculation and the second is a remapping back to the original Eulerian mesh. A unique feature of MESA was the interface reconstruction algorithm. That model allows fewer cells to be used for the same accuracy than in earlier codes because mixed-cell material interface are calculated accurately. A model for ductile and brittle fracture was being developed in 1990 [54] and should have been implemented later. The 3-D MESA hydrocode was developed at the Los Alamos National Laboratory.

3.2.6 HEMP

HEMP is a two-dimensional Lagrangian code, based on a finite difference formulation with a uniform quadrilateral grid. It was used during the seventies and at that time there was no automatic rezoning algorithm for it [55], so severe distortion in the mesh was a problem.

4 Hydrocode simulations

This section contains review of attempts of simulating the behind armour debris, using hydrocodes. The grouping of the reference articles follows the grouping used in the modelling section, with one additional section, of related simulations and numerical models, and additional sub sections. Much of the work done in simulating BAD with hydrocodes considers hypervelocity impacts. The hypervelocity references are collected in a subsection of each section below.

4.1 Target failure and fragment generation

In this section references that have a main focus on target failure and fragment generation are presented.

Al-Hassani *et al* [11] presents a spallation failure model that is applicable to both ductile and brittle materials, since it based on a macroscopic view of the process. The model is incorporated in a not specified hydrocode and shows good agreement when compared with experimental results. The approach to the model is summarized as [11]:

1) A gross damage is defined.
2) The gross damage is evaluated using the conservation and constitutive equations.
3) The model is a simple, non-local damage model based on the physical meaning rather than the numerical method.

A spallation threshold pressure, p_f, is defined in finite difference calculations. This threshold pressure depends on the loading condition. The value of p_f is determined by comparison between numerical and experimental velocity history of the free surface of the target in planar spall tests. In the model it is assumed that the solid constituent is incompressible in the process of damage development. As the damage grows, the generated stress-free surfaces reduce the overall stress. When the gross porosity ϕ reaches a critical value $\bar{\phi}_c$ rapid coalescence of cracks or voids results in complete separation.

The model in [11] only needs two parameters p_f and $\bar{\phi}_c$, which can be determined in comparison between experimental and numerical results. It can be combined with different equations of state and used in 2- and 3-dimensional simulation.

Mescall and Papirno [9] presented criteria for the occurrence of a spall type of fracture under conditions of ballistic impact. Ballistic experiments were performed to assess the predictive values calculated with the HEMP code, with a new spallation criterion incorporated in the code. A damage function K was used and assumed to be a function of the entire stress history.

$$K = \int_0^t (\sigma - \sigma_0)^{\lambda} \, dt \,, \tag{34}$$

Here $\sigma(t)$ is a stress, σ_0 a threshold stress level bleow which no significan damages ocuur regardless of stress duration ($\sigma(t) - \sigma_0 < 0 \Rightarrow K(t) = 0$) and λ a material- dependent parameter chosen to fit experimental data, which gives constraints on the possible values. K is considered to be a measure of damage and to approach a critical value K_{cr} when a specified level of microscopic damage becomes visible at a specific magnification. A set of parameters which gives theoretical

predictions of spall which agree with experimental observations is presented in Table 4 [9]. These parameters were also incorporated in the HEMP code.

Table 4: Spall parameters which agree with experimental data [9].

Steel ANSI 4340 RCH 15	$\sigma_0 = 0.007$ Mbars	$\lambda = 2.0$	$K_{cr} = 337 * 10^{-6}$ Mbar^2 μs
Steel ANSI 4340 RCH 52	$\sigma_0 = 0.020$ Mbars	$\lambda = 2.0$	$K_{cr} = 450 * 10^{-6}$ Mbar^2 μs

The experimental results in [9] verified the predictions of the code to a satisfactory degree. It is notable that when perforation occurred in the experiments a plug was sheared out of the target and it showed evidence of having internal spall.

An attempt to show how SPH can offer significant advantages over traditional (Eulerian and Lagrangian) methods is presented in [56], where EFPs (Explosively Formed Projectile) perforate steel targets. The studied BAD consist of the residual penetrator, eroded penetrator and target material as well as any spallation removed from the target. A main advantage stated in [56] is that due to the meshless Lagrangian formulation, there is no need for the non-physical erosion algorithm normally used in Lagrangian simulations and that mesh distortion is not an issue. The simulations were set up with the SPH processor in AUTODYN 2D and run until all stresses had been relaxed in the residual EFP and the debris cloud. The (smallest) hole diameter in the target plate were measured both experimentally and in the simulations. This is one parameter that can have an influence on the total amount of debris. The prediction was much closer to the experimental values for the thicker plates (20 and 30 mm) than it was for the thin (10 mm) plates. When the problem was remodelled with a smaller particle diameter it gave a better prediction of the hole diameter, thus stating the need of a well chosen problem description. The AUTODYN model is reasonably accurate in predicting the maximum debris cone angle and velocity distribution. The model was unable to replicate the formation of individual fragments, which probably was due to the inability of AUTODYN to model fracture between crystal surfaces [56].

Lynch used the DERA Eulerian code GRIM to assess how well experimental tests could be simulated and to study the way rod and target debris form during penetration [57]. The simulation compares experimental and numerical results for projectile perforation of 100 mm RHA at impact velocities 1550 and 2150 m/s. An analysis of cell size influence was made and shoved 2% change in residual velocity when the cell size was changed from 13 to 10 cells across the projectile diameter. The simulations were conducted both in 2D and 3D. In the two-dimensional case it is clearly stated that the axisymmetry produces fragment rings rather than discrete fragments and that that may give a more narrow debris field than seen in experiments. The 3D code was used for simulations of oblique impact cases [57].

Raftenberg [58] simulated a single experiment with EPIC in order to rectify a previously noted tendency to under-predict target hole size. The slide line erosion feature in EPIC was used to represent penetrator erosion and target hole formation. An erosion-equivalent plastic strain of 1.50 was used. Mie-Grüneisen equations of state were used for all metals. For all metals, a plasticity algorithm was used, with a von Mises yield criterion, the Johnson-Cook yield function, isotropic hardening and radial return. To model damages the projectile was represented with the Johnson-Cook fracture model, while the RHA plate was modelled with four different approaches. The different approaches were:

1. No damage modelling
2. Johnson-Cook fracture model (unmodified EPIC)
3. RHA Constant spall pressure model. This was a model inserted in EPIC by Raftenberg to represent the effect of the phenomena of ductile void nucleation, growth and coalescence into fracture surfaces.

4. RHA Variable spall pressure model. The tensile damage model was modified to represent a hypothesized mechanism of spall pressure reduction in the presence of adiabatic shear bands.

The aim of the simulations in [58] was not to predict behind armour debris, but the hole diameter in the target and the target mass loss were studied. Both are important parameters for the fragment generation.

Numerical simulation of fracture can be carried out in different ways, according to Gulidov [59]. The continuum approach determines the damaged material region and corrects the stress-strain state in that region.

It is, in practical applications, more relevant to trace the origin and development of the fracture process until the body is split into individual fragments. In the case presented in [59], corresponding to the more practically relevant way, two approaches are used:

1. Explicit identification of the crack boundaries in the material.
2. Introduction of discrete particles instead of broken material, which have a finite size, mass momentum and interact between each other and with the boundaries of continuous material.

The second approach is not to be seen as an alternative to the first one, but rather its continuation.

Two models of fracture are presented in [59], one of them based on a local reconstruction of a difference grid. The other employs the substitution of the destroyed material by discrete incompressible particles of finite size.

The difference scheme in [59] is based on approximation of spatial derivates by contour integrals. The distinctive feature of the difference equations for the motions of a node of an individual difference cell from the traditional representation is that the vector of forces acting on the node is represented as the sum of two components, the forces due to internal stresses $\boldsymbol{F}$ and the forces of reaction $\boldsymbol{R}$. The fracture criteria used in [59], combined with a damage parameter, are:

1. maximum tensile stress,
2. maximum tensile strain,
3. maximum shear strain,
4. maximum shear stress,
5. limiting internal energy.

Two methods for identification of the surfaces of continuum violation have been developed. The first one is based on doubling of nodes of the difference grid in the regions of violation of continuum, while the other is based on a local reconstruction of the difference grid in the region where the crack originates.

If a cell with damaged material is located at the computational domain boundary, and the damage achieves the critical value, the material of this cell is substituted by discrete particles. The mass of this cell is distributed among the discrete particles.

To illustrate the capabilities with the model presented in [59] two simulations were conducted, one that clearly shows fragment generation and one that shows plug formation.

A discussion of values for element failure strain, used for erosion algorithms in different hydrocodes, is presented in [60]. To calibrate the values Vignjevic *et al* calculated the penetration depth with an empirical equation and then simulated the same cases with LS-DYNA3D and varied the failure strains until the simulation results were close enough to the empirical. The data used and

gained failure strains are presented in Table 5. It is not specified which material model that was used and therefore can it not be said what the C and *n* in Table 5 represents.

Table 5: Material properites

	Density (ton mm^{-3})	Youngs modulus, *E* (MPa)	*v*	Tensile yield strength, σ_y (MPa)	C (s^{-1})	*n*	Failure strain
Al2024-O (projectile)	2.78E-9	72400	0.33	75	6400	4	1.25
Al5052-O (facesheets)	2.68E-9	70000	0.33	90	6400	4	1.00
Al6061-T6 (extrusion)	2.7E-9	69000	0.33	275	640	4	0.39
Stainless steel, T304	8.0E-9	200000	0.3	290	40.4	5	0.56

In order to verify the values of failure strains determined via the crater depth prediction, they were validated against reported plate perforation studies. This study agreed closely to the experimental values. The material data found were then used in simulations of an aluminium housing sandwiched between two aluminium face-sheets. The housing provided protection for an internal component. This is a rather complicated target, compared to the normal single plate targets, and the behind armour debris should be able to contribute in damaging the protected part. Unfortunately the erosion algorithm was used in such a way that the eroded cells were completely removed form the simulation. This of course results in a loss of total mass and momentum of the simulated system.

4.1.1 Failure and fragment generation in hypervelocity simulations

The hydrocode simulations of hypervelocity impact often focus on fragmentation of the projectile, instead of the target which is the focus of the review. It is nevertheless believed that some techniques may be used for target failure at lower velocities.

Recognizing the potential for improvements in existing particle-based simulation techniques, Fahrenthold and Koo [61] present an alternative energy-based approach to the formulation of particle models for hypervelocity impact simulations. The major drawbacks of the earlier particle methods (conventional particle-in-cell (PIC) and smooth particle hydrodynamics (SPH)) are [61]:

1. Both PIC and SPH use particles that are in fact moving interpolation points and they rely heavily on interpolation theory.
2. PIC methods involve continuous mapping of simulation data between particles and a spatial grid, which can be computationally expensive.
3. SPH methods have been criticized for accuracy and stability problems.

The model presented in [61] can be summarized in the following steps:

1. Specify particle kinematics.
2. Formulate kinetic and internal energy functions for the particle system and describe the non-conservative process of viscous dissipation and heat conduction.
3. Introduce the constraints which govern the mechanical and thermal interaction of the particles.
4. Establish a state space numerical model of the system, by application of Hamilton's canonical equations to the collection of mechanically and thermally interacting particles.

The paper describes the equations needed for two particle-based models, one based on interpolation theory (SPH) and one based on Lagrangian control volumes (called LPH - Lagrangian Particle Hydrodynamics). The described SPH model differs from conventional formulations in its treatment

of space and time varying smoothing distances, while the LPH model differs from both SPH and PIC formulations in its use of deforming mass fixed control volumes to represent the particles. The example simulations with shield perforation were all conducted with thin aluminium shields hit by an aluminium sphere at approximately 7 km/s. Nothing is said about the fragmentation of the shield itself.

Continuing the work by Fahrenthold and Koo [61], Fahrenthold and Horban [62] have developed a hybrid particle-finite element. In the model, particles are used to model contact-impact and volumetric deformation while finite elements represent interparticle tension forces and elastic-plastic deviatoric deformation, simultaneously. The resulting model retains the features of Hamiltonian particle hydrodynamics, while in addition accounting for tensile strength, elastic shearing strain, plasticity and continuum damage effects. There are four ways of element failure in the damage model [62]:

1. The tensile pressure drops below a specific value
2. The effective shear stress exceeds a specific value
3. The maximum eigenvalue of the deviatoric stress tensor exceeds a specific value
4. The accumulated plastic strain exceeds a specific value.

There are failed cells behind the shield in the figures presented in [62], but nothing is mentioned of the behind armour debris characteristics.

The development of the model presented in [62] has continued and among other things new damage models were introduced [63]. The new damage models should respond better to the hypervelocity impact simulation's need of plastic flow, damage evolution and material failure.

Hertel and Kipp have analysed fragmentation of tungsten spheres impacting thin plates at high velocities [64]. They were not primarily interested in the fragmentation of the target plate, but the fragmentation of the impacting sphere itself. This technique may despite this be used for studies of fragmentation of target plates.

The hydrodynamic fracture or spall in CTH is modelled as "void insertion", where the void material is inserted into a computational cell when that cell exceeds a fracture criterion [64]. The results from the simulations were strain rates, average fragment sizes in different regions, where regions of small fragments were associated with high strain rates and visa versa, as well as axial velocity decrease and debris cloud expansion velocities.

4.2 Debris cloud characteristics

The simulations presented in this section are focused on the debris cloud characteristics, but fragment generation is of course dealt with in the simulations despite this focus.

In [65], Mayseless and Yossifon, a numerical calculated fragment distribution is compared with experimental results. It is stated that "The fastest fragments usually emanate from the target material, and they are followed by the eroded projectile. At the back of the cloud a ring of massive fragments, emanating from the target, from around the exit side of the crater, is observed". The experimental debris clouds studied were not hollow, as some models predict them to be.

The AUTODYN 2D Lagrangian processor was used to analyze the spread of BAD when a round nosed Tungsten penetrator perforated a RHA (70 mm thick) target plate. The erosion procedure was used to enable the use of the Lagrangian processor, with criteria determined such that erosion occurred only due to degeneracy of cells.

A typical cloud of debris, according to the numerical simulations, is presented [65, Figure 3], showing the collection of all the nodes associated with fractured cells from both the target and the penetrator. The BAD nodes represent the location, velocity and mass of a cluster of fragments. The correct distribution of fragments inside each fractured cell was calculated from the known state variables (strain rate, temperature etc.) at the time of failure, but neither those calculations nor results are presented in [65]. An interesting result is that there is material that flows into the inner volume of the debris cloud. This was also found in the experimental results used for comparison. When a typical fractured node belonging to the projectile was studied with respect to its radial position and radial velocity history, it was seen that the particle first is moved outwards and later is stopped and moves backwards, towards the axis of symmetry. The forces causing the change in direction are assumed to be elastic forces during the relaxation phase of the crater [65].

The inward motion of fragments within the debris cloud may cause problems when interpreting witness plates, since it is then often assumed that fragments follows a line form the target exit point through a number of witness plates. Many models are also based upon the assumption that the debris only move on an elliptical surface. The problem ought to be negligible at a sufficiently great distance from the target's back surface.

One attempt to simulate BAD using a molecular dynamics approach is presented by Krivtsov in [66]. Here the technique is applied to the macroscopic scale by not considering the particles as atoms or molecules but as elements of the mesoscale level, such as material grains. Two cases of oblique perforation are simulated, one two-dimensional and one three-dimensional. It is stated that wear of the projectile, crater formation, debris sputtering and projectile yaw are in good agreement with experimental results. The material used is modelled as a Lennard-Jones solid, interacting via Lennard-Jones potential.

4.2.1 Debris cloud characteristics in hypervelocity simulations

A model for describing the motion of material in a debris cloud produced by hypervelocity impact of a cylindrical projectile with a thin plate is presented in [67]. The model describes the debris cloud and its motion in terms of impact velocity, projectile mass, material and size, the target material and thickness. Implicit in the model are, among others, assumptions of mass and momentum conservation and that all fragments in the cloud move in straight lines with constant velocity. The motion of the debris cloud structure is described using three-axial velocities V_f, V_I, V_r, a radial velocity V_{rad} and the diameter of the cylindrical projectile d. The three-axial velocities are projectile-target material related, since they are determined by shock-wave interactions, assuming the projectile and bumper discs to be thin enough for one-dimensional shock-wave propagation. A Shock Wave Analysis Program (SWAP) was then used to predict the velocities V_f and V_r, which correlated well with the experiments with which they were compared.

Faraud *et al* [68] report the results of SPH-simulations of debris impact on aluminium target plates. In the simulations were both AUTODYN 2D and PAM-SHOCK 3D used.

Ten simulations, Table 6, were conducted where the debris cloud expansion after a spherical 10 mm projectile perforation of a 2.5 mm thick plate was examined. Both the projectile and the target plate were made of aluminium (Al 6061-T6) and the projectile impact velocities were 7 km/s (hypervelocity).

Table 6: Debris cloud expansion simulation cases [68]

Case	Equation of state	Constitutive relationship	Number of particles in target plate thickness	Coefficients α, β	Smoothing length
1. Autodyn 2D, FV*	Tillotson P_{min}: -1.2 GPa	Steinberg Guinan	10	2.0, 2.0	Not applicable
2. Autodyn 2D, FV*	Shock P_{min}: -1.2 GPa	Steinberg Guinan	10	2.0, 2.0	Not applicable
3. Autodyn 2D, SPH	Tillotson P_{min}: -1.2 GPa	Steinberg Guinan	5	2.0, 2.0	Constant: 2 x (particle diameter)
4. Autodyn 2D, SPH	Tillotson P_{min}: -1.2 GPa	Steinberg Guinan	10	2.0, 2.0	Constant: 2 x (particle diameter)
5. Autodyn 2D, SPH	Shock P_{min}: -1.2 GPa	Steinberg Guinan	5	2.0, 2.0	Constant: 2 x (particle diameter)
6. Autodyn 2D, SPH	Shock P_{min}: -1.2 GPa	Steinberg Guinan	10	2.0, 2.0	Constant: 2 x (particle diameter)
7. Pam-Shock 3D, SPH	Sesame P_{min}: -0.63 GPa	Johnson Cook	5	1.2, 1.5	Variable: Max 0.15 cm
8. Pam-Shock 3D, SPH	Sesame P_{min}: -0.63 GPa	Johnson Cook	5	1.2, 1.5	Variable: Max 0.10 cm
9. Pam-Shock 3D, SPH	Sesame P_{min}: -0.63 GPa	Johnson Cook	10	1.2, 1.5	Variable: Max 0.15 cm
10. Pam-Shock 3D, SPH	Sesame P_{min}: -0.63 GPa	Johnson Cook	10	1.2, 1.5	Variable: Max 0.05 cm

* traditional finite volume technique with erosion algorithm.

The evaluation [68] of the debris cloud expansion agrees with the experimental measures. In all cases the material inside the debris cloud has reached the condition of spalled material at a few microseconds after impact. No influence of equation of state and constitutive relationship on the results relevant to the debris cloud was noted.

Table 7: Debris cloud expansion results [68]

Case	Debris cloud axial position [mm] at 3.6 μs	Debris cloud radial position [mm] at 3.6 μs	Hole diameter in target plate [mm] at 3.6 μs	Debris cloud axial position [mm] at 9.3 μs	Debris cloud radial position [mm] at 9.3 μs	Hole diameter in target plate [mm] at 9.3 μs
1	21.3	12.8	20	57.5	28.8	21.6
2	21.2	12.5	19.3	58.3	26.7	20.7
3	21.6	12.5	≈ 23	56.9	27.0	≈ 26
4	21.2	11.7	≈ 22	55.5	24.4	≈ 25
5	22.0	12.9	≈ 24	58.8	29.7	≈ 27
6	22.3	11.6	≈ 23	58.4	23.7	≈ 26
7	23.5	11.6	≈ 21	57.0 (62.5**)	23.8	≈ 23
8	23.7	11.9	≈ 20	57.0 (63.4**)	23.9	≈ 21
9	23.4	11.7	≈ 20	57.0 (62.0**)	23.9	≈ 23
10	23.3	11.6	≈ 20	57.1 (62.3**)	23.9	≈ 23
Exp.	23	11	21*	58.7	21	21*
* diameter measured on the plate, ** velocity of a few particles						

The paper by Faraud *et al* [68] also presents results where the target consists of three plates. In these cases the agreement between the simulation results and experimental observation was not as good as in the cases with only the first (one) target plate considered. Nothing about the mass distribution within the debris cloud or any separation of target and projectile debris is presented.

A common applications area for SPH techniques is in hypervelocity impact studies related to space structure protection [69]. Hayhurst and Clegg try to reproduce three experimental results using AUTODYN with the SPH and Lagrange processors [69]. The experiments consist of quantified debris cloud characteristics for hypervelocity impacts of aluminium spheres on thin aluminium plates.

The material models for the two aluminium alloys were a Mie-Gruneisen (shock) equation of state and Steinberg-Guinan strength model. A minimum tensile pressure cut-off was used to simulate spalling (12 GPa for both alloys). The simulations cover three cases where the target thickness to projectile (spherical) diameter (t/D) ratio is varied.

Good agreement (within the accuracy of the experimental results) was found when the experimental debris cloud axial velocities were compared to the SPH simulation results [69].

4.3 Combined simulations

There are several models for fragmentation of the target material and several models that describe the characteristics of the debris cloud. There might be a chance to gain the needed results if one of each of those models is combined.

This combination method can also be used when hydrocodes are used. A two step-procedure can be utilised [1]:

1. A well resolved hydrocode calculation of the impact event is performed.
2. The continuum information resulting from the calculations is post-processed to predict the fragment sizes and distribution.

This two-step procedure is used in [1] where AUTODYN2D is used in the first step. Files containing state variables (strain rate, temperature, density etc.) at the time of fracture and debris cloud characteristic (cloud tip and its maximal transversal size) are saved periodically during the simulation. Each and every state variable is accessible via a user sub-routine. The results are checked for new failed cells at each time step during the execution. The state variables for the failed cells are saved together with the history of the debris cloud tip and transversal size. Post-processing of the file with debris cloud data yield the history of bulge development at the target back face, its breakage and the following debris cloud development. The calculation is terminated when the fracture process is completed and the debris cloud is fully developed. Every failed cell is subdivided into four “clusters”. The fragmentation of each “cluster” is determined by the state variables and kinematics at the time of failure of the associated cell and its nodes.

The second step is the post-processing of the data. In [1] this was done with a Matlab program. A typical fragment size for each “cluster” is calculated based on the saved state variables and a physical model. The size distribution is calculated via a statistical model. The global fragment size distribution of the total fragmented mass is gained after accumulation of all distributions for all “clusters”. Further expansion of the nodes associated with failed cells can be determined from simple kinematics.

It was concluded that [1]:

1. The resulting state variables at the moment of fracture, influencing the average fragment size, are insensitive to the details of the specific fracture model chosen, given the total mass loss of both projectile and target materials are the same
2. The fragmentation intensity highly depends on the specific physical model chosen for determination of the average fragment size within each fractured cell.
3. Adding a probability distribution function for the fragment size statistics within each cell yields a more continuous distribution. The cumulative fragment size distribution is insensitive to the details of these fragment size statistics.
4. Comparison of the numerical results with experimental data for the fragment size and global distribution and also for the evolution of the debris cloud indicates that the suggested computational scheme is reasonably accurate.

Further examples of when a two-step method, like the one presented above and in [1], is used can be seen in [70 and 71], where simulations of an 0.3 AP M2 bullet impacting steel plates at velocities about 845 m/s are presented. In [70] three different thicknesses of a high hardness steel (HHS) are considered whilst in [71] three different steel qualities (RHA, HHS and UHH (ultra-high-hardness)) are used as target plates. Of interest in these studies was the fragmentation mass and velocity distribution and the damage incurred by the targets.

A shock equation of state used with a strength model according to Johnson-Cook and a fracture model based on a maximum tensile strain threshold is used for the target in the simulations. The projectile is considered rigid. The material parameters used [70, 71] are presented in Table 8. The results from the experiments and the simulations are presented in Table 9, where "exp" denotes average values from three experiments and "sim" denotes the simulation results.

Table 8: Material proprieties used for simulation in [70] and [71].

	Material	Density, ρ gr/cm^3	Sound speed, c m/s	Shock parameter, s	Gruneisen parameter, Γ	Specific heat, C_p, J/(kg K)	Shear modulus, G GPa	Static flow strength, Y MPa	Strain threshold, ε_f %	Fracture toughness, K_{Ic} $MPa\ m^{1/2}$
Penetrator	St4340	7.85	-	-	-	-	81.8	-	-	-
Target	RHA	7.86	4610	1.73	1.67	477	64.1	930	19	140
	HHS	7.86	4610	1.73	1.67	477	64.1	1550	12	100
	UHH	7.86	4610	1.73	1.67	477	64.1	2000	6	60

Table 9: Results from simulations compared with experimental results.

Target type	Exp vs. Sim	Target thickness (mm)	Impact velocity (m/s)	No. of fragments	Max cone angle (°)	Total fragment mass (mg)
RHA	Exp.	8.0	835	Not found	0	Not found
	Sim.	8.0	835	1	0	617
HHS	Exp.	6.3	844	8	54.7	1039
	Sim.	6.3	846	6	59.6	600
	Exp.	7.9	850	7	68.3	2199
	Sim.	7.9	846	5	66.3	783
	Exp.	10.2	845	3	60.8	1440
	Sim.	10.2	846	4	70.6	898
UHH	Exp.	8.9	836	15	41	2160
	Sim.	8.9	836	8	54	1035

It is, despite the very limited number of experimental results, concluded that the expected increase of the number of fragments with the increase of target hardness was obtained both experimentally and theoretically [71].

Grady and Kipp also used a two-step method [72] when simulating fragmentation of spherical projectiles. During their simulations with CTH a file was written that contained the strain rate, temperature and mass at the time of fracture for each cell. This file was later evaluated in a post-processing mode to define the fragment size and characteristics of the event. The simulations were used to complement and support the interpretation of experimental work. The experiments and presented calculation technique resulted in values of fragmentation toughness, K_f, of some selected materials, Table 10. The simulations captured the axial velocity changes accurately, but over-predicted the deformation of the spherical projectile. Average fragment sizes determined with the simulations appear to be smaller than the dominant size observed in radiographs from the experiments.

Table 10: Fragmentation toughness for selected materials [72].

Material	K_f (MPa m$^{1/2}$)	Material	K_f (MPa m$^{1/2}$)
E52100 Steel	25-45	OFHC Copper	50-80
D6AC Steel	85-105	7075 Aluminum	15-35
AF1410 Steel	85-105	6A14V Titanium	60-90
SS304 Steel	80-100	Tantalum	10-30
APR Steel	55-75		

Verolme and Szymczak [20] did not only develop an analytical model for behind armour debris, they also conducted numerical simulations to gain further results to the model. Tungsten-alloy impact in steel (RHA) was modelled using AUTODYN 2D with the Lagrange processor with the erosion option. The material strength was a Johnson-Cook model. A minimum tensile pressure cut-off was used to simulate spalling. The eroded nodes were retained as translating mass points after erosion. From the simulations cloud frontal velocity, target hole diameter and lateral velocity were obtained. Both the simulated cloud frontal velocity and hole diameter were within 10 % of the experimental values.

Børvik *et al* have used LS-DNYA to simulate ballistic perforation of steel plates [73] to examine if a computational model of viscoplasticity and ductile damage is able to predict a experimentally obtained target response during plugging. The target material was modelled as elastic-viscoplastic with coupled ductile damage. In the simulations the target plate was fully clamped while the projectile was given an impact velocity in the interval ~200 - ~300m/s. The contact between the projectile and target was modelled using a penalty formulation without friction. The agreement between the experimentally and numerically obtained results for plug and projectile exit velocities are very good at the highest simulated impact velocities [73].

Prakash tries to determine the behind armour debris characteristics using the Eulerian code CTH [1, 74]. Two simulations of BAD generated by impact of a generic KE rod on RHA armour of different thickness are presented. In the first simulation the impact is normal and in the second the rod impacts the target with high yaw. The spatial and time distributions of various physical quantities associated with BAD were obtained. One presented quantity is the fragment velocity (in the direction of the initial rod direction) as a function of radial distance from the point of intersection of the line of impact and the targets rear surface.

In the simulations with the yawed rod it was found that the rod exited the target with a lateral shift from the line of initial impact [1, 74]. The debris pattern shows drastic differences from the case with zero yaw. Unfortunately there are no presented mass distribution for the behind armour debris and no material parameters in [1, 74]. The results in [1] are validated by comparison with experimental results for a shaped carge jet perforating a ceramic target. It is stated that the results are "promising", further work are planed to see if CTH can make a better prediction of the fragment distribution within the cone.

Finnegan *et al* [75] used an Eulerian finite difference code, CSQ II, to model the highest and lowest impact velocities studied in an experimental series, where three different target thickness were used. In the experimental study spherical mild steel projectiles, 6.35 mm in diameter, impacted armour steel plates, 1.52, 3.43 and 6.55 mm thick, with impact velocities ranging from 0.21 to 2.09 km/s. The speed ranges were selected to provide impacts above and below the ballistic limit for each target thickness. Therefore only three of the six simulations deal with perforation of the target plate. The results of the simulations are compared with "potted" specimen from the experiments. A "potted" specimen is not intended to represent an exact "freeze frame" at any particular time after impact. It is designed to show the relative positions of the fragments immediately after break-up and to provide an insight into the fragmentation process. In the figures presented in [75] it is clearly seen that at velocities just above the ballistic limit there is only one target fragment, placed as a cap over the projectile, but at higher impact velocities there are several fragments from the target plate.

The agreement between the numerical simulations and the experiments is quite good for the lowest velocities (without perforation) but less precise for the highest speeds. Several reasons for differences between code results and "potted" specimens are given.

Holian [46] has compared experimental results with simulation results, using four different equations of stat (EOS) in the simulations:

1. Tillotson EOS
2. Osborne EOS
3. SESAME 3200 (Barnes-Rod) EOS
4. SESAME 3201 (Holian) EOS

The simulations of a debris cloud produced by the impact of a projectile on a thin metal plate is said to be a good problem to use as a benchmark for testing Eulerian hydrocodes.

In [46], Holian used the Eulerian hydrocode PINON to repeat previously conducted simulations of the debris cloud and adding one further EOS. At first one simulation was compared with an experimental x-ray picture, taken 30 μs after impact. In this case the simulated debris cloud did compare favourably with the experiment. Then the debris clouds were calculated with all four EOSs at 15 μs after impact. The general shape of all debris is the same, however the internal structure and the extent of expansion varies considerably. It is concluded that in accurate hydrodynamic simulations of debris cloud the equation of state can affect the results.

4.3.1 Combined simulations in hypervelocity simulations

A comparison between a spall model and damage models is presented by Geille [76], together with a description of the models.

Spalling is, according to the model, an instantaneous process which occurs in a specific region of the material, depending only on its thermodynamic status, the organization of unloading waves and a specific value of negative pressure.

Damage models are available in two types:

1. Porosity driven:

   These models are based on the replacement of the pressure by a specific variable, porosity, to handle the damage process. This variable contains the information controlling the damage effects (nucleation, growth, coalescence of voids) but no real fragments are created.

2. Sharpnel models:

   Sharpnel models should be used when the composition of the debris cloud is requested. A hydrocode is then used as an advanced "pre-processor" and thereafter shrapnel models, based on statistics, are used to populate the debris cloud.

The Johnson porosity and a spall model are compared in the simulations conducted by Gellie [76], where impact of a thin steel disc flying at 5500 m/s onto a thin steel target is studied. Both models are unphysical in the sense that most of the fragments occupy a fraction of a calculation cell. The cloud composition is directly driven by the mesh generation procedure and the filling algorithm. In the Johnson model the density of the fragments is continuously varying starting from the solid in the back, while the spall model gives an area of constant fragment density. This means that the Johnson model represents a more realistic debris distribution with small softened fragments flying at high velocity in the front of the cloud and larger fragments flying slower behind.

4.4 Simulations for witness pack evaluation

Hydrocode method may as well be used to reduce the number of experiments when threshold curves for metallic witness packs are developed [77]. In [77] AUTODYN was used to model a FSP (Fragment Simulating Projectile). The FSP hit the witness pack with different impact velocities and the residual velocity after the plates within the witness pack was given as result. The material failure of both aluminium and steel was modelled by specifying a maximum strain level. Exceeding this strain level caused the cell to be neglected in the following calculation (numerical erosion). A comparison of experimental data with the numerical results shows that for impact velocities close to the threshold V_{50} the AUTODYN results do not represent reality. This can be explained by the fact that AUTODYN yields deterministic values with no statistical distribution. However the failure modes observed in the simulation agreed with the experimental.

4.5 Other simulations with some relation to BAD

Although this literature review is focused on BAD after perforation of metallic, particularly steel, plates it might be interesting to glance at simulations of other problems as well.

One numerical study where the SPH method in AUTODYN is used is presented by Riedel *et al* [78]. The aim of this study is to gain additional insight and understanding of the physical effects of protective liners behind steel armour. The simulations are compared with experimental results with good agreement. In the simulations the armour steel, projectile and some of the liners were discretised using the SPH-method. The fragment distribution was evaluated equivalently to the experimental procedure in a postprocessor routine.

For the steel target a Mie-Grüneisen equation of state and a Johnson-Cook-strength model was used. Principal strain (ε_{fail}=50%) and principal stress criteria (σ_{fail}=3.8GPa) simulated failure caused by excessive strains and spallation.

Kharchenko *et al* [79] used a finite element code called "IMPRO" to study steel cylinder impact in PMMA (plexiglas) plates of various thicknesses, at low velocities. Analysis of the calculation results shows that in relative thin plates tensile circumferential strains prevail at the plate rear surface. These strains initiate radial cracks when reaching a critical value. For thick plates, the shear strains are the highest and reach a maximum at the plate face in the zone with contact with the projectile.

Tjernberg [80] has simulated armour piercing projectiles penetrating titanium target plates with AUTODYN. The aim of the simulations was to investigate if it is possible to predict the experimentally found V_{50}-velocity for two thicknesses of target plates. In [80] are brief descriptions of the Johnson-Cook strength model and the Johnson-Cook damage model given, as well as the parameters used in the simulations.

A very illustrative figure is presented in [80] and reproduced here as Figure 10. Even though the BAD properties are not of interest in [80] the beginning of fragmentation at the back face of the target is visualized. Fragmentation started when the projectile had penetrated about 81% of the target thickness when the J-C damage model was used, and later when a constant fracture strain of 50% was used. In the simulations (Lagrange formulation) the V_{50}-velocity was underestimated with about 18% when a fracture strain of 25% was used and with about 14% when the J-C damage model was used. The 25% fracture strain is valid for uni-axial tension tests [80].

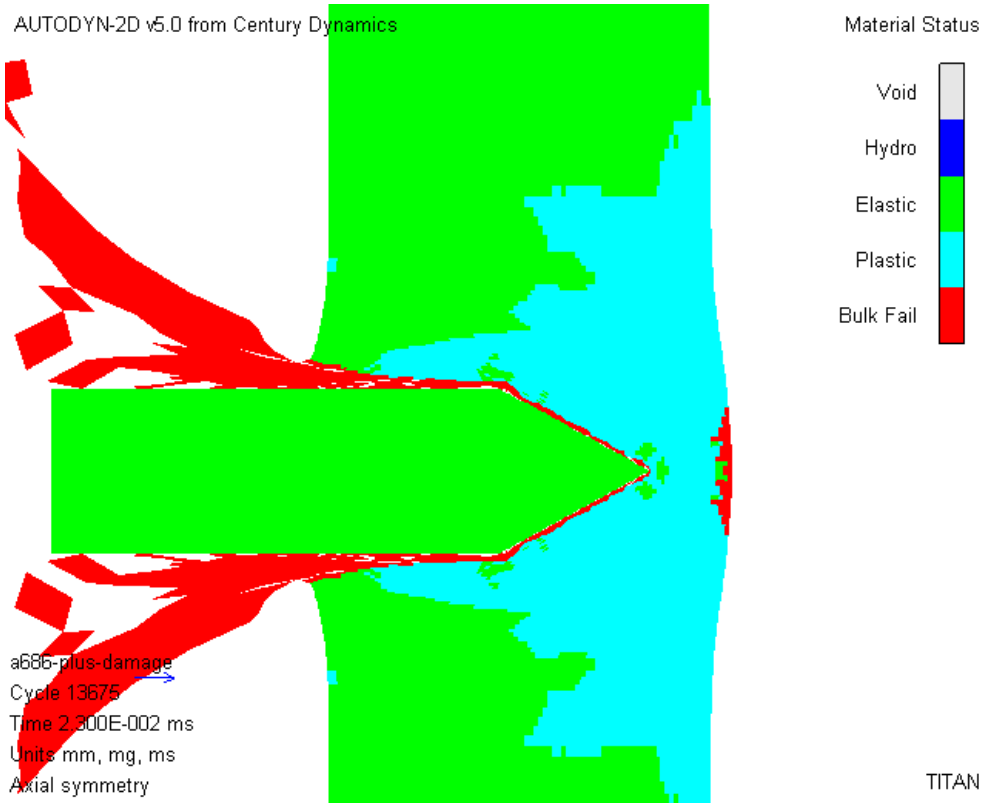

Figure 10: Simulation of AP projectile penetrating titanium target [80]

Another study that did not consider fracturing of the target plate, but nevertheless stated the importance to simulate it is Yoo's numerical simulations where steel spheres impact thin steel plates [81]. The study represents computations for oblique impact of mild steel spheres onto stationary mild steel thin plates, using a Lagrangian code, NET3D. The prediction of sphere deformation and ricochet is in good agreement with experimental findings, even at high obliquity, while the prediction of ballistic limits differ somewhat. The discrepancy in ballistic limit is believed to be due

to different failure mechanisms. In the experiments, the primary failure mode involves the formation and expulsion of a central plug by shear failure processes, while in the simulations plate perforation mainly relies on the element erosion associated with the plastic strains. Better agreement was indicated at increased obliquity, because the failure pattern changes from plugging to petaling [81].

Gou *et al* [82] discuss the use of shell elements to model panel-like targets in perforation simulations, using LS-DYNA. The numerical examples in the paper include the performance of conical and flat nosed projectiles. By comparing the simulation results from finite element models where the targets are modelled by shell elements and 3-D solid elements, respectively, they state that shell element modelling can save much computational time and also produce good results. A criterion for the validity of modelling a panel-like target by shell elements is proposed:

$$\frac{D_p \sigma_{yp}}{h \sigma_{yt}} > 15.0, \tag{35}$$

where D_p is the projectile diameter, h the target thickness, σ_{yp} and σ_{yt} are the yielding strengths of the projectile and target materials, respectively.

A major difference between the capacity of a 3-D solid element and a 2-D shell element lies in the stress states of the material [82]. The normal stress along the "thickness" direction in a shell element is basically neglected, resulting in an element type that can not account for stress wave propagation in the thickness direction of the target. When the influence of normal stress on target failure cannot be ignored one has to use the solid elements [82]. However, when the perforation is dominated by annulus failure or shear band plugging, the shell elements could be able to model the material failure.

In the conducted simulations element erosion was used to remove elements that reached a specific equivalent plastic strain. Nothing about detached elements can be found in [82] and therefore the applicability for BAD-simulations is not known.

Gee has conducted computational experiments for the perforation of thin oblique steel plates by L/D 10 tungsten-alloy projectiles with CTH [83, 84]. Primary simulation parameters included impact pitch angle, number of target plates and impact velocity. The behind armour debris was not analyzed directly but its influence is mentioned in connection with a discussion of perforation efficiency of a second target plate. It is stated that it is possible that the penetration in the second target plate is initiated by the debris rather than the residual projectile. The figures in [83 and 84] clearly show material removed from the target and projectile, probably as a result of eroded cells.

Dzwinel *et al* [41] used a molecular dynamic approach to study the penetration of a semi rigid rod in a solid argon target in the micro scale (l~10^{-7}m). The simulations were conducted with two different impact velocities 200 m/s and 1000 m/s where the projectile was rigid with the lower velocity and eroded with the higher. The article discusses the penetration process, including the shape of the hole depending on the projectile nose shape and the erosion process, and compares the result and physics with simulations in the macroscopic scale. The projectile never perforates the target, but in one case the target material cracks around the projectile and at the back surface, where a bulge also is formed.

In another paper, also presenting only penetration without perforation examples, Camacho and Oritz [85] depart from the continuum damage theories and investigate the feasibility of accounting explicitly for individual cracks as they nucleate, propagate, branch and possibly link up to form

fragments, a feature that not is avaible in moste other hydrocodes. The paper presents a model with its system representation, equations of motion, contact algorithm, thermal effects, constitutive model, fracturing and comparison with experiments. In the model, cracks are allowed to form and propagate along element boundaries in accordance with a cohesive-law model. It is up to the mesh to provide a rich enough set of possible fracture paths, which can be arranged with adaptive meshing, but not implemented in the model [85]. New surfaces are created as required by the cohesive model by duplicating nodes along previously coherent element boundaries.

One further model for fracture modelling is presented by Olovsson and Unosson [86]. The model is an engineering model based on a probability to find a defect with a smallest size in an arbitrary volume of the target plate, where the defect distribution is a target material parameter. The model is intended for the finite element code KRYP, which is a program for meso-mechanical crystal plasticity simulations developed at FOI, the Swedish Defence Research Agency [87].

The model [86] attempt to handle two problems can occure in combination of crack propagation in continumm mecanincs and finite elemtent analyses:

1. Variations of materials will, in a statistical way, make small volumes capable of larger deformations than larger volumes.
2. Cracks are normaly wery sharp, but no perfect singularities. A coarse element net will not be able to to represent the local geometry and deformation gradients around the crack tip, which will under estimate the tensions. On the other hand, the local deformations will be oversteimated, if the crack is prepresented with eroded cells in a net that is finer than the real crac tip radius. This means that the fracture energy will converge to zero as the element sizes are refined.

Olovsson and Unosson [86] have two engineering ways to cope with these problems:

1. A random distribution of defects in the material creates a physical motivated size dependencie within the material.
2. The dependence of element size is compensated by scaling of the rate of tensional deformation for elements at the tip of the crack.

Ågårdh and Laine [88] conducted simulations of steel projectiles perforating reinforced concrete slabs. The simulations were carried out with the LS-DYNA hydrocode and a material model which includes erosion.

A failure surface, expressed either as the second invariant of the deviator stress tensor J_2 or as the stress difference $\Delta\sigma = \sqrt{3J_2}$, was computed based on normalised test data. Only one quarter of the slab and projectile was modelled, thus using two symmetry planes. Eight node solid elements were used for all parts included.

The erosion option was based on plastic strain. Erosion occurred in the concrete when the pressure reached a failure pressure limit. Tensile fracture is described with a pressure cut-off value.

In these simulations the eroded cells were removed and there are thus no debris ejected from the back face of the concrete slab. Nevertheless the simulations give clear indications of the number of cells removed due to spalling at the back face of the slab.

Another problem is studied by Inaoka and Takaysau [89, 90]. They present a model of a three dimensional impact fracture process based on a competitive process of fragments, where the fragmentation of the material is initialized at the impact end.

It is stated that when an object undergoes an impact, many cracks appear near the impacted surface and propagate to the opposite side. The crack propagation front, called a failure wave, forms a plane-like shape that propagates with nearly constant velocity, v_0, and most of the fragmentation occurs on the front. Since the wave is plane is it possible to convert the three dimensional problem into a two dimensional problem. The crack density decreases as the wave propagates, meaning that the fragments at the impact surface are finer than the ones near the opposite side. It also assumed that the cracks do not bifurcate. With the dilation field and a spatial fluctuation in the elastic moduli the randomness of the material is incorporated in the model. Simulations with the model give that the cumulative mass of the fragments follows a power law

$$P(\geq m) \propto m^{-\tau}, \qquad \tau = 0.66. \tag{36}$$

The value of $\tau = 0.66$ is very close to ⅔. Such exponent value have been observed in many experimental studies [89,90].

5 Discussion

Modelling penetration, perforation and BAD is necessary in assessment of vulnerability and survivability. Despite the well-recognised need it is hard or even impossible to find a suitable model for the generation and distribution of this kind of fragments. One other possible use of BAD modelling can be in design of spall liners, which are mounted in military vehicles to reduce the effects of BAD, and thus increase the survivability of the personnel if the vehicle is hit. In this case the BAD modelling should give the liner designer a better foundation of what strains the liner should be able to handle.

Many models only cover parts of the complete process. It might be possible to connect two or more models to gain a combined complete model, but there will probably be problems of interoperability between the models. The usual needs of experimentally obtained parameters will still be a major problem. To be able to rely on the results the simulations may have to be restricted to one or a few material combinations and velocity regimes, where experimental sources can be found. There is always a possibility to conduct new experiments, but that will in many cases be quite expensive, and it can be hard to reproduce experiments. The objective with simulations is often to perform analyses more cheaply than an experimental study and to be able to vary parameters. Howerver, can the results be trusted when the parameters are varied?

The generation of multiple fragments from the target (in opposition to plug formation, “one fragment”) are described as two phenomena, either spalling, due to tension stress waves in the material, or crushing of the material in front of the penetrator. Both phenomena are probably involved in the actual fragment generation process, but most models only handle one of them. No reference of the relative importance of these two different origins of debris has been found. The so-called ring fragments, which often are found in experimental studies, are normally neglected in the models. This may be acceptable since they normally have low velocities, but on the other hand; these types of fragments are rather large and thus important in mass conservation analyses.

Statistical methods, which often need experimental results to calibrate parameters, are often used to model the mass distribution and velocities of the separate fragments. Some models, proven with experimental results, predict the fragments emerging from the back face of the target to be larger than those emerging from within the target. It is also believed that a projectile that impacts with an impact velocity just above the perforation velocity causes fewer fragments than a faster projectile. A positive feature with statistical methods is that they embody the stochastic behaviour found in experimental studies. Part of the stochastic behaviour is probably due to a random distribution of inhomogeneities within the target material. The material properties are not known in such detail that this can be modelled without a statistical distribution of the inhomogeneities when the problem is analyzed in more global view.

A common approach in modelling BAD cloud characteristics is to assume that fragments are positioned on an expanding elliptical surface. Evaluation of such models compares well with flash X-ray photos of the cloud. However it should be interesting to see results from an experimental study where only a slice of the cloud is allowed to travel away from the target and to be recorded on film. This kind of experiment would show whether the interior of the cloud is as empty as basic assumptions predict it to be. There is one study that shows fragments that have an inward (towards the shot-axis) motion. The basic assumption of many models may be too coarse a simplification of the reality if this is correct. One other problem that arises is the interpretation of witness plates. On the other hand the inward motion will probably be restricted to a volume very close to the target since there will not be any driving forces once the fragment has left the target. The problem can then be neglected, if the evaluations of cloud size or witness plates are conducted at a sufficient distance from the target.

Those using hydrocodes to simulate the BAD phenomena encounter other difficulties. There is much research work at hand just for simulation of the penetration phase, without subsequent perforation. Damage evolution is hard to simulate and there is also the problem of material properties at the very high strain rates in the ballistic perforation process. One other problem in the numerical simulations is the finite size of the computational cells, which might be larger than a typical size of a fragment.

A seemingly useable approach is to use the hydrocode as a pre-processor and then take the results from it and use within another code which uses a statistical distribution of fragment sizes, directions and velocities. The numerical erosion procedure can be used to decide when a cell is damaged in such a way that it should be considered by the post-processor in this case.

The hydrocodes and other numerical models often have a powerful graphical presentation processor. This is an enormous strength as well as a great danger. The result looks so good and trustworthy, that an inexperienced reader/user easily forgets the hidden assumptions and simplifications. One example of such figures is the BAD created in 2D simulation, where the displayed "fragments" often are fragment clusters that should be considered as circular rings around the axis of symmetry.

Regardless how the BAD is modelled, either via a physical model or numerically with a hydrocode, one has to have access to experimentally found BAD characteristics. The phenomena seem to be so hard to model that without comparing the model results with the experimentally found results the model should not be used. It is unfortunately very hard and expensive to get the experimental results needed.

This review clearly shows that simulation of behind armour debris generation and distribution is a hard task. There are more or less complete models presented in the open literature, but to use them and write a computer code based on the model, is in many cases almost as hard as to design a new model. When thinking of using a model found in the open literature, or to design a new one, one has to consider the intended application of the model. Conservation of energy and mass will be essential if the aim is to better understand the fracture and fragment distribution processes in detail. On the other hand, if the model only shall estimate the BAD cloud in a "simple way", with a statistical distribution, it might be enough to require that the energy is conserved on the average in multiple simulations of the same case, to a good enough degree or even not to consider the conservation requirements at all.

The conclusions by Dinovitzer *et al* [6] seem still to be valid to a great extent:

1. Additional work is still required in understanding the underlying physics of behind armour debris generation.
2. An integrated behind armour debris characterisation and modelling process has not yet been fully developed.

To be able to better understand the behind armour phenomena is it probably necessary to conduct well-instrumented experimental studies and simulate the same cases. The amounts of model and simulation comparisons with experimental results are in some model presentations very limited. Due to the stochastic nature of fragment generation it is probably necessary to perform several experiments, which are expensive, to catch average values of BAD characteristics. At least these average values should be possible to reproduce with models and other numerical simulations if the models are good enough. It will be even better if the stochastic phenomena are incorporated within the models.

In order to get a model or simulation procedure to gain the information needed for assessment of vulnerability and survivability one has to use a model that handles all phases of the process, from initial penetration, via a perforation and fragment generation phase, until and including the free flight of the fragments and the residual projectile. At this moment it is possible to know if a component or a person within the protected platform will be hit, and if so what mass and velocity the hitting fragment will have. There will, however, be one major problem remaining: How to asses the damage the fragment can cause to the object it hits.

Much of the work presented is in the hypervelocity regime, which is far above the impact velocities involved in kinetic energy projectiles impacting military targets. Such work is nevertheless reviewed in order to point out the methodology.

6 Conclusions

It is obvious that modelling and simulation of BAD still needs much research activities, especially in order to be useful in vulnerability assessments. Most models and simulations efforts deal only with parts of the problem, either fragment generation or BAD cloud characteristics. There is a large number of models that predict spall, but very few that handle fragmentation and still fewer that include the ring fragment often seen in experiments. A drawback of many models is the need of experimentally determined parameters, since this can make them inaccurate when new material combinations are to be modelled.

The numerical simulations have their own problems. Material fracturing is harder to simulate than deformation without fracture. When material is detached from the back face of a target plate it is not with a continuous mass distribution, but dependent on the size of the computational cells. One shall not expect to get a correct result from a hydrocode, just by defining the problem and starting the simulation. Much knowledge and understanding of the model has to be gained before, and in most cases the hydrocode will only deliver a nominal result, thus not being able to include the stochastic behaviour of fragment generation. Numerical erosion is sometimes used to predict the amount of fragments generated during the penetration and perforation process, and the eroded cells are then post-processed in a separate program. This is a possible way to consider the stochastic behaviour and gives a chance to adjust the mass distribution within the fragments, according to some statistical distribution.

A first combined experimental and numerical study could focus on the parameters given in Table 11. When this is done for the first combination of material type and projectile type other materials and projectile types have to be examined as well.

Table 11: Parameters to vary in experimental and numerical studies

Series	Projectile type	Impact velocity	Target material	Target thicknes
1A	Rigid	Constant	Constant	Varying
1B	Rigid	Constant	Varying hardness	Constant
1C	Rigid	Varying	Constant	Constant
1D	Rigid with varying calibre	Constant	Constant	Constant
1E	Rigid, oblique impact	Constant	Constant	Constant

The parameters to study should be:

1. Total mass of fragments from the target plate
2. Mass distribution of the fragments
3. Velocity and direction of flight for the fragments
4. Velocity of the projectile before impact and after perforation
5. Target plate mass loss

When the numerical results can be compared with an experimental study such as the one described above there should be a good possibility to adjust parameters so that other simulations also will be reliable.

7 References

1 A. Parkash, Virtual experiments to determine behind-armor debris for survivability analysis, U.S. Army research Laboratory, Survivbility/Lethality Analysis Direcotorate
http://www.asc2004.com/Manuscripts/sessionF/FP-09.pdf accesed 2005-06-24
2 G. Yossifon, A. L. Yarrin, Behind-the-armor debris analysis, International Journal of Impact Enginering 27 (2002) 807-835
3 A. S. Dinovitzer, M. Szymczak, M. Steele and I. F. Glen, Characterization of Behind-Armour Debris, 16TH International Symposium on Ballistics
4 Y. Baillargeon, M. Szymczak, A. S. Dinovitzer, T. Brown and B. Xu, Major Issues Affecting Characterisation and Modelling of Behind-Armour Debris, 19TH International Symposium of Ballistics, 7-11 May 2001, Interlaken, Switzerland
5 J. A. Teland, Multifunctional numerical tool for penetration analysis, FFI/RAPPORT-2002/04647, Norwegian Defence Research Establishment, P O Box 25, NO-2027 Kjeller, Norway
6 A. S. Dinovitzer, M. Szymczak, T. Brown, Behind-armour debris modeling, 17th International Symposium on Ballistics, Midrand, South Africa, 23-27 March 1998
7 M. E. Backman, W. Goldsmith, The mechanics of penetration of projectiles into targets, Int. J. Engng. Sci., 1978, Vol. 16, pp. 1-99
8 T. Autoun, L. Seaman, D. R. Curran, G. I. Kanel, S. V. Razorenov, A. V. Utkin, Spall Fracture, Springer-Verlag New York, 2003, ISBN 0-387-95500-3
9 J. Mescall, R. Papirno, Spallation in Cylinder-Plate Impact, Experimental Mechanics, 257-266, July 1974
10 A. Dinovitzer, Debris Characterisation and Modelling (DeCaM) Software Improvments, Final Report, August 1999, Defence Research Establishment Valcartier, Canada
11 S.T.S Al-Hassani, D. Chen, M. Sarumi, A simple non-local spallation failure model, Int. J. Impact Engn, Vol. 19, Nos. 5-6, pp. 493-501, 1997
12 D. E. Grady, Local inertial effects in dynamic fragmentation, J. Apll. Phys. 53(1), January 1982
13 D. E. Grady, The spall strength of condensed matter, J. Mech. Phys. Solids Vol. 36, No. 3, pp. 353-384, 1988
14 J.R. Klepaczko, P. Chevrier, A meso-model of spalling with thermal coupling for hard metallic materials, Engineering Fracture Mechanics 70 (2003) 2543-2558
15 L. C. Chhabildas, L. M. Barker, J. R. Asay and T. G. Trucano, Relationship of fragment size to normalized spall strength for materials, Int. J. Impact Engng. Vol. 10, pp. 107-124, 1990
16 S. J. Bless, Spall criteria for several metals, University of Dayton, Research Institute, Dayton, Ohio, June 1981
17 D. Chen, Y. Yu, Z. Yin, H. Wang, G. Liu, On the validity of the traditional measurement of spall strength, International Journal of Impact Engineering 30 (2005) 811-824
18 J. Liss, W. Goldsmith and J. M. Kelly, A phenomenological penetration model of plates, Int. J. Impact Engng. Vol.1, No.4, pp.321-341, 1983
19 A. Pytel, N. Davids, A viscous model for plug formation in plates, J. Franklin Inst. 276 (1963) 394-406
20 J. L. Verolme and M. Szymczak, Behind-armour debris modeling for high-velocity fragment impact, 17th International symposium on ballistics, Midrand, South Africa, 23-37 March 1998
21 M. Held, Fragment Mass Distribution of "Secondary Fragments", Propellants, Explosives, Pyrotechnics 16, 21-26 (1991)
22 AVAL Reference manual, FMV Swedish Defence Materiel Administration, 2004
23 G. Wijk, Sharp-Nosed Projectile Perforation of Target Plates, FOA-R--99-01106-310--SE, April 1999, ISSN 1104-9154
24 M. Mayseless, N. Sela, A. J. Stilp, V. Hohler, Behind the armor debris distribution function, 13th International Symposium on Ballistics, Stockholm, Sweden , 1-3 June 1992
25 V. Hohler, K. Kleinschnitger, E. Schmolinske, A. Stilp, K Weber, M. Mayseless and N. Sela, Debris cloud expansion around a residual rod behind a perforated plate target, 13th International Symposium on Ballistics, Stockholm, Sweden , 1-3 June 1992
26 R. Saucier, R. Shnidman, J. C. Collins III, A stochastic behind-armor debris model, 15th International Symposium on Ballistics, Jerusalem, Israel, 21-24 May, 1995
27 A. J. Piekutowski, Effects of scale on debris cloud properties, International Jounal of Impact Engineering, Vol. 20, pp. 639-650, 1997
28 A. S. Dinovitzer, M. Szymczak and D. Erickson, Fragmentation of targets during ballistic penetration events, Int. J. Impact Engng Vol. 21, No. 4, pp. 237-244, 1988
29 A.L. Yarin, I.V. Roisman, K. Weber, V. Hohler, Model for ballistic fragmentation and behind-armor debris, International Journal of Impact Engineering 24 (2000) 171-201
30 G. Wijk, Secondary BAD (Behind Armour Debris) from projectile perforation of target plates, FOA-R--99-01245-310--SE, October 1999, ISSN 1104-9154, FOA Defence Research Establishment, SE-147 25 Tumba, Sweden
31 L. A. Merzhievsky, Statistical characteristics of a debris cloud behind a shield, , Int. J. Impact Engng. Vol. 20, pp. 569-577, 1997
32 AUTODYN Theroy manual, Revison 4.3, Centry Dynamics

33 K. Thoma, W. Riedel, F. Schäfer, S.Hiermaier, Status and perspectives in protective design, Space Debris 2, 201-224, 2000
34 R. D. Cook, D. S. Malkus and M. E. Plesha, Concept and applications of finite element analysis, Third edition, John Wiley & Sons 1989, ISBN 0-471-84788-7
35 Y. C. Fung, P. Tong, Classical and Computational Solid Mechanics, World Scientific, 2001, ISBN 981-02-3912-2
36 A. Ghali, A. M. Neville, Structural Analysis; A Unified Classical and Matrix Approach, Third Edition, Chapman and Hall, 1989, ISBN 0-412-29040-5
37 E. W. Weisstein, Finite volume method, From MathWorld -- A Wolfram Web Resource. http://mathworld.wolfram.com/FiniteVolumeMethod.html
38 D. R. Scheffler and J. A. Zukas, Practical aspects of numerical simulation of dynamic events: material interfaces, International Journal of Impact Engineering 24 (2000) 821-842
39 S. Hiermaier, Numerische Simulation von Impaktvorgängen mit einer netzfrien Lagrangemethode (Smooth Particle Hydrodynamics), ISSN 0944-8381, Universität der Bundeswehr München, 1996
40 L. D. Libersky, A. G. Petschek, T. C. Carney, J. R. Hipp and F. A. Allahdadi, High strain Lagrangian hydrodynamics; A three-dimensional SPH code for dynamic material response, Journal of Computational Physics 109, 67-75 (1993)
41 W. Dzwinel, W. Alda, J. Kitowski, J. Moscinski, D. A. Yuen, An examination of long-rod penetration in micro-scale using particles, Journal of Materials Processing Technology 60 (1996) 415-420
42 T. Belytschko, Y. Krongauz, D. Organ, M. Fleming and P. Krysl, Meshless methods: An overview and recent developments, Comput. Methods Appl. Mech. Engrg. 139 (1996) 3-47
43 J.-P. Ponthot, T. Belytschko, Arbitrary Lagrangian-Eulerian formulation for element-free Galerkin method, Comput. Methods Appl. Mech, Engrg. 152 (1998) 19-46
44 T. Belytschko, Y. Y. Lu, L. Gu and M. Tabbara, Element-free Galerkin methods for static and dynamic fracture, Int. J. Solids Structures Vol. 32, No. 17/18, pp. 2547-2570, 1995
45 R. Shivarama and E. P. Fahrenthold, An ellipsoidal particle-finite element method for hypervelocity impact simulation, Int. J. Numer. Meth. Engng 2004; 59:737-753
46 K. S. Holian, Hydrodynamics code calculations of debris clouds produced by ball-plate impacts, International Journal of Impact Engineering Vol. 10, pp. 231-239, 1990
47 C. J. Hayhurst, S. J. Hiermairer, R. A. Clegg, W. Riedel, M. Lambert, Development of material models for Nextel and Kevlar-Epoxy for high pressures and strain rates, International Journal of Impact Engineering 23 (1999) 365-376
48 D. Post, Codes Written by the National and International Computational Physics Community, LA-UR-02-6284, Los Alamos National Laboratory
49 G. R. Johnson, R. A. Stryk, T. J. Holmquist and O. A. Souka, Recent EPIC code developments for high velocity impact: 3D element arrangements and 2D fragment distributions, Int. J. Impact Engng. Vol. 10, pp. 281-294, 1990
50 W. S. de Rosset and A. B. Merendino, Radial hole growth: Experiment vs Calcualation, Eighth international symposium on ballistics, Orlando, Florida, October 23-25, 1984
51 W. J. Flis, Fully automatic rezoning for a finite-element hydrocode in 2-D and 3-D, 17th International symposium on ballistics, Midrand, South Africa, 23-27 March 1998
52 J. M. McGlaun, S. L. Thompson, M. G. Elrick, CTH: A three-dimensional shock wave physics code, Int. J. Impact Engng. Vol. 10, pp. 351-360, 1990
53 Information from www.lstc.com, accessed 2005-03-21
54 D. J. Cagliostro, D. A. Mandell, L. A. Schwalbe, T. F. Adams and E. J. Chapyak, ;MESA 3-D calculations of armor penetration by projectiles with combined obliquity and yaw, Int. J. Impact Engng. Vol. 10, pp. 81-92, 1990
55 G. R. Johnson, A new computational technique for intense impulsive loads, Third international symposium on ballistics, Karlsruhe, Federal republic of Germany, 23-25 March 1977
56 M. W. Dalzell, P. J. Hazell and J. H. Meulman, Modelling behind-armour debris formed by the perforation of an EFP through a steel target, 20th International symposium on ballistics, Orlando, Florida, 23-27 September, 2002
57 N. J. Lynch, Constant kinetic energy impacts of scale size KE projectiles at ordnance and hypervelocity, International Journal of Impact Engineering 23 (1999) 573-584
58 M. N. Raftenberg, Target tensile damage and strength effects in steel plate perforation by a small length-to-diameter ratio tungsten projectile, 16th International symposium on ballistics, San Francisco, Ca, 23-28 September, 1996
59 A. I. Gulidov, V. M. Fomin, I. I. Shabalin, Mathematical simulation of fracture in impact problems with formation of fragments, International Journal of Fracture 100: 183-196, 1999
60 R. Vignjevic, K. Hughes, E. A. Taylor, Finite element modelling of failure of a multi-material target due to high velocity space debris impacts, Space Debris 2, 41-50, 2002
61 E. P. Fahrenthold and J. C. Koo, Energy based particle hydrodynamics for hypervelocity impact simulation, Int. J. Impact Engng. Vol. 20, pp. 253-264, 1997
62 E. P. Fahrenthold, B. A. Horban, A hybrid particle-finite element method for hypervelocity impact simulation, International Journal of Impact Engineering 23 (1999) 237-248
63 E. P. Fahrenthold, B. A. Horban, An improved hybrid particle-element method for hypervelocity impact simulation, , International Journal of Impact Engineering 26 (2001) 169-178

64 E. S. Hertel, Jr. And M. E. Kipp, Numerical fragmentation modeling and comparisions to experimental data, 19th International symposium of ballistics, 7-11 May 2001, Interlaken, Switzerland
65 M. Mayseless and G. Yossifon, Behind armor debris: Fragments distribution, 18th International symposium on ballistics, San Antonio, Texas, 15-19 November, 1999
66 A. M. Krivtsov, Simulating perforation of thin plates using molecular dynamics approach, Proceedings of International Conference "Shock waves in Condensed Matter", St.-Petersburg, Russia, 2000, 158-160
67 Andrew J. Piekutowski, A simple dynamic model for the formation of debris clouds, Int. J. Impact Engng. Vol. 10, pp. 453-471, 1990
68 M. Faraud, R. Destafinis, D. Palmieri, M. Marchetti, SPH simulations of debris impacts using two different computer codes, International Journal of Impact Engineering 23 (1999) 249-260
69 C. J. Hayhurst, R. A. Clegg, Cylindrically symmetric SPH simulations of hypervelocity impacts on thin plates, International Journal of Impact Engineering, Vol. 20, pp. 337-348, 1997
70 M. Ravid, G. Yossifon, S. R. Bodner and R. Keren, Characterization of the fragmentation exit failure mode and fragment distribution upon perforation of metallic targets, 20th International Symposium on Ballistics, Orlando, FL, 23-27 September 2002.
71 G. Yossifon, M. Ravid, R. Keren, S. R. Bodner, Characterization of the fragmentation exit and fragmentaion distribution upon perforation of metallic targets of different hardness, 21st International Symposium on Ballistics, Adelaide, Australia, 19-23 April 2004
72 D. E. Grady, M. E. Kipp, Fragmentation properties of metals, International Journal of Impact Engineering, Vol. 20, pp. 293-308, 1987
73 T. Børvik, M. Langseth, O. S. Hopperstad, K. A. Malo, Ballistic penetration of steel plates, International Journal of Impact Engineering 22 (1999) 855-886
74 A. Prakash, Determining behind-armor debris characteristics by 3-D computer simulations, 20th International symposium on ballistics, Orlando, FL, 23-27 September, 2002
75 S. A. Finnegan, J. C. Schulz, O. E. R. Heimdahl, Fragmentation characterization techniques for ordnance speed impacts, 10th International Symposium on Ballistics, October 27-28-29, 1987 San Diego, California
76 A. Geille, Numerical modeling of damage in various types of hypervelocity experiments, International Journal of Impact Engineering 23 (1999) 271-281
77 J. L. Verlome, M. Szymczak and J. P. F. Broos, Metallic witness packs for behind-armour debris characterization, International Journal of Impact Engineering 22 (1999) 693-705
78 W. Riedel, K. Weber, M. Wicklein, K. Thoma, J. Färber, Reduction of fragment effects behind layered armour - experimental and numerical analysis, 21st International Symposium on Ballistics, Adelaide, Australia, April 19-23, 2004
79 V. V. Kharchenko, A. L. Maistrenko, A. I. Babutskii, Impact deformation and fracture mechanism of plates of brittle materials, Strength of Materials, Vol. 34, No. 3, 2002, pp. 269-272
80 A. Tjernberg, Penetration simulations of titanium plates, FOI-R--1315--SE, September 2004, ISSN 1650-1942, Swedish Defence Research Agency, Weapons and Protection, SE-147 25 Tumba, Sweden
81 Y.-H. Yoo, Numerical simulation of oblique impact of mild steel spheres against mild steel thin plates, 20th International symposium on ballistics, Orlando, FL, 23-27 September, 2002
82 J. Guo, G. Shi, Y. Wang, C. Lu, Efficient modelling of panel-like structures in perforation simulations, Computers and Structures 81 (2003) 1-8
83 D. J. Gee, Oblique plate perforation by slender rod projectiles, 19th International symposium of Ballistics, 7-11 May 2001, Interlaken, Switzerland
84 D. J. Gee, Plate perforation by eroding rod projectiles, International Journal of Impact Engineering 28 (2003) 377-390
85 G. T. Camacho, M. Oritz, Computational modelling of impact damage in brittle materials, Int. J. Solids Structures Vol. 33, No. 20-22, pp. 2899-2938, 1996
86 L. Olovsson, M. Unosson, Brottmodellering av hårdmetall i KRYP, (Fracture modelling of hard metall in KRYP), FOI-R--1306--SE, September 2004, ISSN 1650-1942, Swedish defence research agency, SE-147 25 Tumba, Sweden.
87 L Olovsson, KRYP, a Finite element Tool for Crystal Plasticity Analyses, FOI-R--0374--SE, March 2002, ISSN 1650-1942, Swedish Defence Research Agency, SE 147 25 Tumba, Sweden
88 L. Ågårdh, L. Laine, 3D FE-simulation of high-velocity fragment perforation of reinforced concrete slabs, International Journal of Impact Engineering 22 (1999) 911-922
89 H. Inaoka, H. Takayasu, Universal fragment size in a numerical model of impact fracture, Physica A 229 (1996) 5-25
90 H. Inaoka, H. Takayasu, Application of statistical physics to impact fragmentation, Physica A 274 (1999) 300-309

Appendix 1: Summary of reviewed models

Table 12 shows a summary of some of the details some of the reviewed physical, empirical and statistical models handles. The models are created with different purpose and therefore presented in different ways, whereby some information may be neglected. It is nevertheless believed that Table 12 shows the main characteristics of the models.

Table 12: Summary of reviewed models.

Model	Rigid projectiles	Eroding projectiles	Fragmentation (according to Figure 3)	Spallation (according to Figure 3)	Ring fragments	Fragment nominal mass / size	Fragment mass / size distribution	Fragment velocity distribution
Al-Hassani *et al* [11]				Yes[1]				
Chhabildas *et al* [15]				Yes[1]			Yes	
Dinovitzer *et al* [28]	Yes[2]		Yes			Yes	Yes[1]	
Fugelso and Blodedow[3] [7]			Yes	Yes				
Grady [12]			Yes	Yes		Yes		
Grady [13]				Yes		Yes		
Held [21]							Yes[1]	
Klepaczko and Chevrier [14]				Yes				
Liss *et al* [18]	Yes					Yes[4]		Yes
Mayseless *et al* [24]		Yes	Yes[1]		Yes	Yes[5]	Yes[5]	Yes
Merzhievsky [31]							Yes	Yes
Mescall and Papirno [9]				Yes[1]				
Pytel and Davids [19]	Yes					Yes[4]		
Saucier *et al* [26]							Yes[1]	Yes
Verolme and Szymczak [20]						Yes	Yes	Yes[1]
Wijk [30]	Yes	Yes	Yes[6]	Yes[6,7]	Yes[6]	Yes[1,6]	Yes[1,6]	Yes[6]
Yarin *et al* [29]		Yes	Yes			Yes	Yes	Yes

[1] Requires experimental results.
[2] Also for obliqe impact.
[3] As presented in the review by Backman and Goldsmith [7].
[4] Single plug.
[5] Mass per unit angle.
[6] Not compared with experimental results.
[7] Only for the ring fragments.

Appendix 2: Abbreviations

2D	Two dimensional
3D	Three dimensional
ALE	Arbitrary Lagrangian-Euler
AP	Armour Piercing
BAD	Behind Armour Debris
DEM	Diffuse Element Method
DREV	Defence Research Establishment Valcartier
e.g.	for example
EFG	Element Free Galerkin
EFP	Explosively Formed Projectile
EOS	Equation Of State
Eq	Equation
FSP	Fragment Simulating Projectile
HHS	High Hardness Steel
KE	Kinetic Energy
LPH	Lagrangian Particle Hydrodynamics
MD	Molecular Dynamics
PIC	Particle-In-Cell
PMMA	Ppolymethylmechacrylate
RHA	Rolled Homogenous Armour
SPH	Smooth Particle Hydrodynamics
UHH	Ultra-High-Hardness
V/L	Vulnerability / Lethality